Aus der Klinik für Allgemein-, Viszeral- und Transplantationschirurgie
der Ludwig-Maximilians-Universität München
Leitung: Prof. Dr. med. Jens Werner

Dissertation
zum Erwerb des Doctor of Philosophy (Ph.D.)
an der Medizinischen Fakultät der
Ludwig-Maximilians-Universität zu München

Establishment of an Endoscopy-Guided minimally invasive murine orthotopic colorectal cancer model

vorgelegt von
Chen Chen
aus
Jining, China
2021

Mit Genehmigung der Medizinischen Fakultät der
Ludwig-Maximilians-Universität zu München

Betreuer:	**Prof. Dr. Alexandr V. Bazhin**
Zweitgutachter:	**PD Dr. med. Tobias Schiergens**

Dekan:	**Prof. Dr. med. dent. Reinhard Hickel**

Datum der Verteidigung:

19.10.2021

Parts of this work have been published in:

Chen Chen, Jens Neumann, Florian Kühn, Serene Lee, Moritz Drefs, Joachim Andrassy, Jens Werner, Alexandr V. Bazhin, Tobias S. Schiergens*

“Establishment of an Endoscopy-guided Minimal-invasive Orthotopic Mouse Model of Colorectal Cancer”

published in *Cancers* (2020)

DOI: 10.3390/cancers12103007

Table of contents

Abstract

Colorectal cancer (CRC) is a major health problem worldwide and the second leading cause of cancer mortality. Murine CRC models play an important role in related research and the most widely used orthotopic model represents an open surgical model (OSM) using laparotomy. However, the OSM requires advanced surgical skills and creates surgical traumas. Thus, this study aimed to establish an endoscopy-guided minimally invasive model (EGM) to overcome the inherent defects of the OSM and then compare it to the OSM. Murine CRC cell lines including CT26 and MC38 were implanted into BALB/c and C57BL/6J mice, respectively. Follow-up colonoscopy was conducted weekly in the EGM group. In all animals, gross as well as microscopic examination including Hematoxylin and eosin staining and immunohistochemical staining as well as assessment of immune cell infiltration were performed. A score of cell injection performance, procedure duration and adverse event rates were recorded to analyze the learning curve characteristics of both models. In the EGM, the presence of colorectal wall infiltration, luminal ulceration, lympho-vascular invasion, tumor-infiltrating lymphocytes were detected, as well as spontaneous lymph node, peritoneal and hepatic metastases, while primary submucosa infiltration was detected in the OSM, due to surgically injected tumor cells originated from the subserosal layer. The primary tumors from both groups showed cytoplasmic immuno-staining for Cytokeratin 20. Compared to the OSM, the EGM required less time (11.95 ± 5.07 min vs. 33.73 ± 5.24 min, $P < 0.001$), and less advanced surgical skills according to the performance score (1.79 ± 1.12 vs. 2.25 ± 1.29, $P = 0.006$),

in addition, in EGM, the adverse event rate and the experience level demonstrated a significant negative relation ($r = -0.237$, $P = 0.002$), in OSM, Only the rate of wound dehiscence was significantly reduced to 0 after the first 20 procedures ($P = 0.003$), abdominal adhesions with bowel obstruction / ischemia was independent of technical procedural factors. In conclusion, when compared to the OSM, the presented EGM is able to mimic human CRC more closely and tumors can be minimal-invasively and longitudinally monitored via colonoscopy. It is easy to learn and can be established quickly and safely.

List of tables

List of figures

Abbreviations

ATCC	American Type Culture Collection
BLI	Bioluminescence imaging
CIMP	CpG island methylator phenotype
CK20	Cytokeratin 20
CRC	Colorectal cancer
DMEM	Dulbecco's Modified Eagle Medium
DPBS	Dulbecco's phosphate-buffered saline
DSMZ	Deutsche Sammlung von Mikroorganismen und Zellkulturen GmbH
DSS	Dextran sodium sulfate
EGM	Endoscopy-guided model
FBS	Fetal bovine serum
GEMM	Genetically engineered models
H&E	Hematoxylin and eosin
IHC	Immunohistochemistry
MRI	Magnetic resonance imaging
MSI	Microsatellite instability
OSM	Open surgical model
PET-CT	Positron emission tomography–computed tomography
RPMI	Roswell Park Memorial Institute Medium
SD	Standard deviation
TILs	Tumor-infiltrating lymphocytes

1. Introduction

1.1 Colorectal cancer

Colorectal cancer (CRC) is the fourth most common cancer (after lung, breast and prostate cancers), more worryingly, the second leading cause of cancer-related mortality worldwide. It was accounted for approximately 10% of total cancer cases and 8.5% of all cancer deaths in 2018 (1).

1.1.1 Tumorigenesis of CRC

CRC is a disease of modernity. The highest incidence is mainly found in developed countries and the number of CRC patients is increasing in countries undergoing economic growth (2). Risk factors include genetic predisposition, high-fat diet, obesity, tobacco smoking, large intake of red and processed meat, alcohol consumption, and certain forms of micriobial dysbiosis (3-13).

Both colon and rectum consist of four layers: the mucosa, the submucosa, the muscularis propria and the serosa. As the inner lining of the colon and rectum, the mucosa is made up of the epithelium (a thin layer of columnar epithelial cells), the lamina propria (a layer of connective tissue) and the muscularis mucosa (a thin layer of muscle). The epithelium of the normal colon and rectum undergo continuous renewal, and the crypts which are finger-like invaginations consisting of columnar epithelial cells are the places for cellular reproduction. The adenomas is known as benign outgrowths of epithelium, and adenocarcinomas which account for most CRC are characterized by malignant glandular

epithelial cells invading through colorectal wall layers (muscularis mucosa, sumbumosa, muscularis propria), 10%-20% adenocarcinomas may show a mucinous component (14). Various assumptions have been proposed for CRC development and progression, and the adenoma-carcinoma sequence (adenomatous pathway) is widely accepted as the classic description of colorectal carcinogenesis based on several studies, it was demonstrated as follows: dysplastic adenomas are the most common form of premalignant precursor and can eventually acquire invasive potential (15-19). The multistep process of CRC is based on APC gene mutation, KRAS gene mutation and inactivating mutations of the TP53 gene, the characteristic genetic changes are often accompanied by chromosomal instability (CIN). And major molecular alterations of the serrated pathway include BRAF gene mutation, microsatellite instability (MSI) and CpG island methylator phenotype (CIMP) (12, 14, 20).

1.1.2 Mechanisms and challenges of metastasis

CRC patients without metastasis have a high chance to be cured, however, 40%-50% of all CRC patients either develop synchronous (at the time of initial diagnosis) or metachronous (in the course of their disease) metastasis (21, 22). In order to better determine a patient's prognosis and the course of treatment, cancer staging system was introduced and the UICC 8th edition TNM staging system (Figure 1) of the International Union Against Cancer (UICC) is now the globally recognized standard for CRC staging (23-26). In this staging system, "T" is defined as the local extent of the primary tumor, "N" refers to the status of the regional lymph nodes and "M" is used to describe distant

metastasis (27).

Figure 1. UICC TNM staging of CRC (26).

Metastasis is the process whereby cancer cells spread throughout the body from a primary site, to a distant organ. It consists of sequential, interlinked and selective steps which include: primary tumor growth, angiogenesis, epithelial-to-mesenchymal transition (EMT), invasion, intravasation, survival in circulation, extravasation, dormancy and secondary tumor growth at the distant site. The EMT process provides stationary and polarized epithelial cells with motility which has been revealed to play a critical role in epithelium-derived carcinomas metastasis. During EMT process, stationary and polarized epithelial cells lose their cell–cell adherence and apical–basal polarity, thus acquire certain mesenchymal characteristics such as enhanced migratory capacity, invasiveness and elevated resistance to apoptosis. In CRC, EMT has been revealed to play a critical role in epithelium-derived carcinomas metastasis (21, 28, 29).

While some variability exists on the organs of metastasis among patients with different kinds of cancers, it is well known that particular cancers have propensity to form metastases in specific organs (organotropism). CRC typically metastasizes to the liver (most frequent site of metastasis) and/or lung (30). The theory behind the organ-specific pattern of metastasis has not been fully understood yet. Currently, the generally accepted explanations are that the portal drainage of the colorectal blood is partially responsible for the high rate of liver metastasis as well as the “seed and soil” hypothesis proposed by Stephen Paget (31). According to that the non-random pattern of metastases forms only when the seed (affinity of certain tumor cells/tissues) and soil (the milieu of a certain organ) are compatible.

As in many other cancer types, prognosis of CRC patients is determined by metastatic

tumor progression in the majority of the cases (1, 32, 33). This emphasizes the significance of distant spread in CRC and the need for research on its mechanisms in order to target this process in a therapeutic setting. Indeed, the major barrier lying in CRC treatment is metastasis, and several key questions still remain unanswered. As issues like the role of host microenvironment, the entry and proliferation of disseminated or circulating tumor cells, the characteristics of the “seed” cells and the “soil” (secondary organ) or the mechanisms controlling metastatic dormancy remain unsolved, metastasis related studies on the systemic, cellular and molecular levels are highly imperative for cancer research.

1.2 Mouse models of colorectal cancer metastasis

While improvements of *in vitro* or *ex vivo* models such as cell lines and organoids have contributed a lot to CRC research, these strategies are limited by lack of host microenvironments (34). Therefore, *in vivo* models still play an indispensable role in CRC progression, metastasis, interaction with the immune system and drug resistance (35). The mouse and human exhibit certain similarities regarding genetics, anatomy and physiology, therefore over 95% of animal studies are conducted in mice (36, 37). CRC develops along the large intestine consisting of colon, and rectum. Murine and human large intestines share the same microscopic mural structure including mucosa, submucosa, inner circular and outer longitudinal tunica muscularis and serosa layers (38). In general, murine CRC models can be grouped as genetically engineered and implantation models, and a variety of CRC metastasis models have been generated since

mouse models of CRC were introduced 80 years ago (39-41).

1.2.1 Genetically engineered models

The genetically engineered mouse models (GEMM) offer the potential to study a particular gene during carcinogenesis, however, its high costs, the long latency of tumorigenesis in combination with a short lifespan due to growth of small bowel tumors and other extra-colorectal manifestations limit their application in CRC research, for instance, the widely used Apc mutant mice. Some researchers claimed that unlike the implantation models, GEMM enable *de novo* tumor progression without interference of tumor cell / tissue from outside, which may even more closely resemble human CRC. However, metastasis was rarely observed in GEMM models which makes this model less suitable to study mechanisms of distant spread (42-55).

1.2.2 Implantation models

In implantation models, tumorigenic cells or tissues are inoculated, e.g. injected, into the murine host. This might involve the inoculation of human (xenograft) or murine (syngeneic / allograft) cells, organoids or tissues (56).

1.2.2.1 Implantation materials

Many CRC cell lines have been developed since CRC cells were firstly implanted in mice in the 1960s (53), for instance, Caco-2 cells (57), HT29 (58), LS174T (59), SW48 (60), SW620 (60), which are all derived from CRC patients. Murine CRC cell lines are also available, common examples include MC38 cell line from C57BL/6 mice and CT26 cell

line from BALB/c mice, in detail, the MC38 murine cell line was derived from a grade III colon adenocarcinoma in a female C57BL/6 mouse which was induced by repeated carcinogen 1,2-dimethylhydrazine dihydrochloride injection subcutaneously, the murine CT26 cell line was developed from a grade IV undifferentiated colon carcinoma in a female BALB/c mice by repeated rectal administration of the carcinogen N-nitro-N-methylurethane (61-63).

Although tumor cell line injection is technically easy to perform and of low costs, these cell lines may be genetically far away from their origin due to prolonged *in vitro* passaging, Thus, tumor fragments either from biopsies or previously grown tumors were used to overcome this problem, briefly, they are usually cut into 1mm cubes and sutured onto the cecal or colonic wall (64). This strategy avoids the changes of tumor cell characteristics and represents the inherent heterogeneity of spontaneous CRC, but it is labor intensive and sometimes limited by availability of tumor specimens (40).

The encouraging development of three-dimensional organoids could improve those patient-derived xenograft models. Organoids are three-dimensional structures consisting of different organ-specific cell types generated exclusively from the culture of primary tissues or embryonic / induced pluripotent stem cells using similar processes as occurred *in vivo*, including self-organization and spatially-restricted lineage commitment (65-67). Currently, CRC organoid culture is available from both human and murine tissues, and implantation of organoid is feasible (35, 68, 69).

1.2.2.2 Implantation methods

1.2.2.2.1 Orthotopic models

In orthotopic CRC tumor models, tumorigenic material, most often cells, is implanted into the colorectal wall of the host (53). Several models feature spontaneous distant metastasis.

1.2.2.2.1.1 Open surgical technique

The open surgical model (OSM) is the most commonly used method in murine CRC and many of these models show distant spread. Usually the cecum is exteriorized following laparotomy and represents the implantation site with the aim of primary tumor growth. Generally the cecum is easy to identify because of its sudden increase in bowel diameter (70). The higher tumor take rate involved in cecum compared to other parts of colon is another reason to choose this region as implantation site, just as lower rates of death due to intestinal obstruction and the technical possibility to surgically remove tumors to study the hosts response (71).

1.2.2.2.1.1.1 Tumor cell line implantation

The first murine CRC orthotopic implantation model was established in 1977 (72) where 10^6 MCA-38 cells were injected into the distal colon, proximal colon, and cecum of a male C57BL/6 mouse, respectively. The lowest tumor take rate was found in the proximal and distal colon, while the highest was observed in the cecum (90%). Half of the animals developed macroscopic liver and mesenteric lymph node metastases 8-9 weeks after injection. From then on, the cecum injection technique has been widely adopted. However,

in the majority of reports, injection was performed into the serosal / subserosal layers which does not refer to the original origin of CRC (69, 73-81).

Alencar *et al.* (82) established a murine CRC model with injection in the mucosal and submucosal layers of the cecum by creating a 1cm bowel loop in the transverse colon and a 2.5cm bowel loop in the descending colon using nontraumatic clamps, before cell suspension injection, 0.05% trypsin in EDTA was injected into the bowel loops and incubated for 30min to facilitate tumor cell implantation. Fourteen days after implantation, tumorigenesis occurred in all mice.

Cespedes *et al.* injected HCT116, SW620 and DLD-1 into the cecal wall following laparotomy (83). The primary tumor take rates of the three cell lines were 75%, 75% and 88%, respectively. The presence of lymph node, liver and lung metastases were also studied. For the HCT116 group, the dissemination rate was 100% (lymph nodes), 67% (liver) and 50% (lung). In the SW620 group, all mice developed tumor foci in lymph nodes, 17% of mice had lung metastasis, while no tumor was found in the liver. In the DLD-1 group, the dissemination rates were 57% (lymph nodes), 29% (liver) and 29% (lung).

Terracina *et al.* injected CT26 cells into the submucosal layer of the cecal wall using a 1mL syringe with a 28G needle after cecotomy (84). On day 23 after injection, 23 out of 26 mice had developed tumors, and all 23 mice developed mesenteric lymph node metastases.

1.2.2.2.1.1.2 Tumor tissue implantation

Rashidi *et al.* (85) obtained colon tumor tissue from a patient with poorly differentiated adenocarcinoma, one or two fragments ($1mm^3$) were implanted into the cecum of

recipient mice, where a small area of the cecal serosa was removed in advance. Extensive multilobe liver metastases were detected in all mice on day 10 postoperatively, and all lymph lodes draining the liver developed metastasis by day 19.

Jin *et al.* (86) harvested tumor tissue from a LoVo cell line induced subcutaneous CRC model on male BALB/c nu/nu nude mice. Then a colostomy was performed in the cecum of 14 nude mice, and tumor fragments were sutured into the submucosa of the stoma. The ostomy healed 2 weeks postoperatively, 12 mice developed tumors 3 weeks after implantation, 3 mice had mesenteric lymph node metastasis while no metastases were found in lung or liver.

In another study by Seguin *et al.* (87) a piece of CT26 tumor tissue was sutured onto the cecal wall after serosa removal just as the procedures conducted by Endo *et al.* (88). The BALB/c Mice developed primary tumors (ranging from 15 to 20mm^3) on day 5, however, the exact tumor take rate and incidence of metastases were not shown.

1.2.2.2.1.1.3 Organoid implantation

O'Rourke *et al.* engrafted colorectal shApc organoids into the colon mucosa of Athymic-Nude-Foxn1^{nu} mice (89). The implantation method was adapted from a protocol for the engraftment of APC-inactivated intestinal organoids (90). In brief, transient colonic injury was induced by DSS to create a niche facilitating organoids implantation. It was revealed that 62% of mice developed tumors 7 weeks after implantation and macroscopic liver metastases in 1 out of 6 mice were identified 21 weeks after implantation.

Fumagalli *et al.* (68) used intestinal carcinoma organoids derived from VillinCreER^{T2}::AKP genetic mice. In this study, an epithelial pouch was created by disruption of the muscularis

layer of the recipient mice. ThAKP organoids led to a 100% (N=22) primary tumor take rate and metastasis formation rate.

1.2.2.2.1.2 Minimal invasive transanal model

Although the tumor take rate of OSMs can be very high and thus these models very effective, several researchers claimed that surgical stress may lead to decreased immune function, especially natural killer cell suppression. This might provide a tumor-friendly environment and act as a confounder regarding tumor growth and immunogenicity and limit the reliability and feasibility of future research goals of measuring immune responses after tumor resection (82, 91-93). Moreover, young-onset CRC are more common in the distal large intestine defined as distal to the splenic flexure (including the descending colon, sigmoid colon and rectum) (94), while the majority of OSMs mainly focus on the proximal large bowel defined as colon segments proximal to the splenic flexure. This makes it less suitable for research on young-onset and distally located CRCs (95, 96). The introduction of models with transanal injection techniques could overcome these problems since they not only feature distal tumor locations but also represent non-operative techniques requiring shorter operation time and recovery time for mice. This might result in less technical complications such as bowel obstruction or ischemia due to adhesions as well as less blood loss (84, 97).

1.2.2.2.1.2.1 Traditional trans anal implantation techniques

Kashtan *et al.* (98) transanally injected CT26 cells, MCA38 cells and LS174T cells into the rectal submucosa with a 30G needle. Tumors developed in 87.2% of mice (41/47); in detail, 17 out of 22 mice and 20 out of 20 mice in the animal group with murine cell

injection (CT26 and MCA38, respectivelly) and in 4 out of 5 mice with the human tumor cell line LS174T. While lymph node metastases were only found in 8.5% of all cases (4/47) this was limited to the CT26 group, and no metastases were detected in MCA38 and LS174T groups.

Donigan *et al.* (93) injected CT26 cells into the rectal submucosa using a 29G syringe under a magnification of ×100 as described in a previous study (99). A tumor incidence of 65% and a rate of distant metastasis of 3.3% were reported in this study.

Except tumor cell lines, tumor tissues can also be implanted transanally. Enquist *et al.* (100) collected 10mm^3 tumor fragments, which were derived from HCT116 / LS174T human CRC cell line induced subcutaneous CRC model on NOD/SCID mice, and sutured the tumor fragments onto the rectal mucosa using 4-0 Vicryl sutures. Primary tumors were detected via colonoscopy, and lymph node, hepatic and pulmonary metastases were found 3 weeks (HCT116 group) and 8 weeks (LS174T group) after implantation.

1.2.2.2.1.2.2 Enema technique

Takahashi *et al.* induced short time colitis by dextran sulfate sodium (DSS) in nude mice followed by transanal LS174T cell instillation (101). They noted a 95% tumor incidence in the animals' rectum 2 weeks after instillation while metastasis was not found.

Kishimoto H *et al.* used a similar technique (102) with application of acetic acid solution to disrupt the epithelium of the rectal mucosa. Subsequently, CT26 cells and HCT-116 cells were instilled transanally. All mice developed rectal tumors, lymph node and pulmonary metastases were found in over 90% of mice.

The application of inflammatory agents such as DSS and acetic acid facilitated the

induction of rectal tumors at high incidence, suggesting that inflammation enhances tumor formation in the mucosa (89, 101). Meanwhile, differing from other CRC models in which tumors form in the submucosa and serosa layer, those tumors were growing on the surface of the mucosa where human CRC originates. However, this technique limits the tumor to the rectum and the massive inflammation represents a rather artificial and confounding aspect in this model.

1.2.2.2.1.2.3 Electrocoagulation technique

Bhullar *et al.* (103) used transanal low dose mucosal electrocoagulation of the colorectum followed by human (LS174T cells and HT29 cells) and murine CRC cell (CRL2638 cells and CRL2639 cells) instillation, respectively. It was revealed that for the group of animals with human cell line injection, the tumor take rates were 58% (HT29 group) and 100% (LS174T group), respectively. Lymph node and distant metastasis were detected in 10 out of 12 and 4 out of 12 mice with HT29 and LS174T, respectively. For the group with murine cell injection, the tumor take rates were 100% (CRL2638 group) and 92% (CRL2639 group), respectively, while lymph node and distant spread were detected in 12 out of 12 and 6 out of 12 mice with CRL-2638 cell line and CRL-2639 cell line injection, respectively.

1.2.2.2.1.2.4 Endoscopy-guided minimally invasive model

In humans, endoscopy is the most important strategy for CRC screening, diagnosis and follow up care (104). This technique has been adapted to be used in small animals, i.e. mice for research purposes (105). In 2005, Alencar *et al.* used a fiber optic flexible endoscope to detect and characterize CRC tumors in mice (82). Later in 2005, Becker *et al.* introduced the Coloview® system (Karl Storz, Tuttingen, Germany) as tool for rigid

endoscopy in mice (106). The authors published detailed protocols for colon pathology evaluation, biopsy sampling and methylene blue staining (107). Since then, endoscopy has become more and more popular to study CRC in mice (108-115). The advantages of this technique include the possibility of chromoendoscopy which enables the discrimination between neoplastic and inflammatory changes of the murine colon, in addition, CRC progression can be successively monitored with high resolution colonoscopy as well as biopsy sampling which was shown to be sufficient for histological and molecular analyses without sacrificing animals (106, 107).

In the setting of murine CRC injection models, the use of endoscopy to inject tumorigeneic cells into the colorectal wall was previously reported. Zigmond *et al.* (105) employed the Coloview® system to implant human CRC cell lines (SW620, SW480, LS174T) and the murine CRC cell line MC38 into the colonic submucosa. Tumor incidence was 100% in surviving mice (95%), while distant metastases were not detected. The same Coloview® system was also used by Bettenworth *et al.* (116) for human CRC cell line HT-29 implantation into NOD/SCID mice. Marked colonic tumors were detected from day 12 after implantation, 36 days after implantation, 28.6% of all mice developed liver metastases and 14.3% of all mice developed peritoneal metastases. Zhao *et al.* (117) also used the Coloview® system for microinjection of CT26, HT29, and MC38 cells. Four weeks after injection, tumor growth was only detected in the HT29 group.

Except for tumor cell lines, tumor organoids can also be implanted with the help of endoscopy. Both mouse and patient derived tumor organoids were delivered to the distal colon mucosa by Roper *et al.* using optical colonoscopy (118, 119). For murine tumor

organoids, at week 12 after injection, 15 primary tumors and 3 liver metastases were observed in 10 mice. For patient-derived primary CRC organoids, 24 primary tumors were revealed 8 weeks after injection and 8 liver metastases were found 12 weeks after injection. In addition, bioluminescence imaging (BLI) and fluorescence imaging techniques were also used to track primary tumor and metastasis.

1.2.2.2.2 Models of distant metastasis

Mouse models with the specific aim to achieve distant metastasis often involve the injection of tumorigeneic cells directly into the systemic circulation. Since liver (approximately 50% of CRC patients) (120) and lung (approximately 5-15% of CRC patients) (121) metastases are the most common sites for distant spread, spleen, portal vein and liver parenchyma are often used as injection sites, whereas tail vein injection is performed to achieve lung metastasis (53, 122). Although this technique is very fast, effective and reproducible in inducing metastasis, it bypasses the steps of primary tumor growth with subsequent distant spread thereby eliminating the early stages of the metastatic cascade.

Review of the available CRC models suggests that the optimal models of human CRC never exist, different kinds of models focus on various research aims by means of mimicking different parts of CRC tumorigenesis. Therefore, it is of vital importance to choose models according to different research proposes, and within the framework of currently used model, its relative limitations should always be taken into consideration in order to analyze data meticulously. In addition, more efforts should be made to develop

CRC models which can mimic human CRC more comprehensively and accurately without endangering ethics.

1.3 Study aims

The aim of the present study was to establish two murine orthotopic CRC injection models, the OSM and the EGM. Based on a comprehensive literature research on both techniques, we hypothesized that (1) the EGM is easier and faster to establish as compared to the OSM, (2) the EGM can more accurately emulate the patterns of primary tumor growth of CRC as compared to the OSM based on the injection layer of the colorectal wall, (3) the use of endoscopy enables the longitudinal evaluation of CRC development thereby reducing the animals' sample size and thus following the 3R principle of animal research. Thus, the specific aims of the study were:

(1) To establish a minimally invasive murine orthotopic EGM of CRC using the Coloview® system.

(2) To establish an OSM with injection into the cecal wall as referenced gold standard of orthotopic CRC models.

(3) To compare these models regarding establishment performance (learning curve characteristics), primary tumor growth and distant metastasis.

(4) To compare the characteristics of tumorigenicity and immunogenicity of two murine CRC cell lines (MC38 and CT26) being injected in both models, respectively.

2. Materials and Methods

2.1 Ethical framework

This study was approved by the responsible animal care committee (ROB-55.2-2532.Vet_02-17-110). All experiments were performed in compliance with the guidelines for animal protection in Germany and those of the Federation of European Laboratory Animal Science Associations (123). Cervical dislocation was used for animal euthanasia. We followed the ARRIVE guidelines for reporting *in vivo* studies (124).

2.2 Mice

BALB/c mice and C57BL/6J mice aged 10-11 weeks (Charles River, Sulzfeld, Germany) were housed in temperature and humidity-controlled rooms (22 ± 2°C, 55 ± 5%) at the Walter Brendel Centre of Experimental Medicine (LMU, Germany). The animals were housed in groups of five in a Makrolon® type II cages (Tecniplast Deutschland GmbH, Hohenpeißenberg, Germany) containing low-dust softwood fiber bedding material. Cage bedding change was performed weekly. One red, transparent plastic play tunnel, one red, transparent plastic igloo and nesting material were provided in each cage for animal enrichment. Animals were maintained in a 12-hour light / dark cycle, provided with normal pelleted mouse chow food (ssniff Spezialdiäten GmbH, Soest, Germany) and tap water *ad libitum*. Mice were allowed to acclimatize to the housing conditions and husbandry procedures for at least one week prior to the experiment.

2.3 CRC cell lines

Murine CRC cell lines CT26 (American Type Culture Collection (ATCC), Manassas, VA) which was generated from BABL/c mice was cultured in Roswell Park Memorial Institute medium (RPMI1640, Gibco, Paisley, UK) with 10% fetal bovine serum (FBS, BIOWEST, Nuaillé, France) and 1% penicillin-streptomycin (pen-strep, PAN-Biotech, Aidenbach, Germany) and MC38 which was generated from C57BL/6 mice, it was a gift from the Wolf Lab (Gene Center and Department of Biochemistry, LMU) and was cultured in Dulbecco's modifed Eagle's medium (DMEM, Gibco, Paisley, UK) with 10% FBS and 1% pen-strep. Both cell lines were incubated in a 5% CO_2 incubator (Binder GmbH, Crailsheim, Germany) at 37°C. CT26 was authenticated by the IDEXX BioAnalytics (Ludwigsburg, Germany) and MC38 was authenticated by Deutsche Sammlung von Mikroorganismen und Zellkulturen GmbH (DSMZ, Braunschweig, Germany) before experiments. PCR-based mycoplasma testing was performed at regular intervals (quarterly) on all cell lines used. Cells in the log phase were collected using trypsin (Biochrom GmbH, Berlin, Germany) and single-cell suspensions were prepared using Dulbecco's Buffered Salt Solution (DPBS, PAN-Biotech, Aidenbach, Germany) and kept on ice.

2.4 Cell proliferation and cell viability analyses

Cell proliferation was examined using EZ4U cell proliferation assay (Biomedica Medizinprodukte GmbH, Vienna, Austria) according to manufacturer's instructions. Briefly, 100µL cell suspension (4×10^3 cells) were seeded into each well of 96-well microtiter plates and grown for specified time periods (12, 24, 36, 48, 72, 84 and 96h). Subsequently,

cells were treated with dye solution for 2h in 37°C incubator. After incubation, the plate was removed from the incubator. Absorption was measured at both, 450nm and 492nm with 620nm as a reference on a VersaMax Microplate Reader (Molecular Devices, Biberach an der Riss, Germany).

CASY cell counting technology was used to evaluate cell viability, only aliquots with a viability of at least 90% were injected. Cells in the log phase were collected and suspended in DPBS at required densities (10^4/50µL, 2×10^5/50µL, 2×10^6/50µL) and then kept on ice. Before implantation, the viability was determined using the CASY Cell Counter & Analyser System (OLS OMNI Life Science, Bremen, Germany) according to the manufacturer's instructions.

2.5 Experimental groups

In a prospective study, the study aims specified in 1.3 were tested by experiments using 216 mice overall. The outcome measures determined by the study included establishments of both EGM and OSM; comparison of the two models regarding establishment performance (learning curve characteristics), primary tumor grwoth and distant metastasis; comparison of the characteristics of tumorigenicity and immunogenicity of two murine CRC cell lines (MC38 and CT26) being injected in both models, respectively.

The number and distribution of mice in each experimental group are shown in Table 1. A subgroup size of four animals was granted by the animal care committee. Animals were allocated into treatment groups by randomly picking numbers out of a box and the groups

were indicated using cage labels. The researcher establishing models and evaluating results (i.e., injection of cells, administration of analgesic agent, performing tumor volume measurement, etc.) was unaware of the allocation of treatment groups which was implemented by masking cage labels before each treatment session. Blinding procedures of the OSM was limited by obvious abdominal sutures.

Table 1**.** Experimental subgroups of the EGM and OSM using with different cell numbers for injection as well as observation periods.

	Group		Number of cells	Number of animals		Observation period (weeks)
				Female	Male	
EGM[A]	Experimental group	1.1.1	10^4	2	2	1
		1.1.2		2	2	2
		1.1.3		2	2	3
		1.1.4		2	2	4
		1.2.1	10^5	2	2	1
		1.2.2		2	2	2
		1.2.3		2	2	3
		1.2.4		2	2	4
		1.3.1	10^6	2	2	1
		1.3.2		2	2	2
		1.3.3		2	2	3
		1.3.4		2	2	4
	Negative control[B]	1.4.1	0	1	1	4
OSM[A]	Experimental group	2.1.1	10^4	2	2	1
		2.1.2		2	2	2
		2.1.3		2	2	3
		2.1.4		2	2	4
		2.2.1	10^5	2	2	1
		2.2.2		2	2	2
		2.2.3		2	2	3
		2.2.4		2	2	4
		2.3.1	10^6	2	2	1
		2.3.2		2	2	2
		2.3.3		2	2	3
		2.3.4		2	2	4
	Negative control[B]	2.4.1	0	1	1	1
	Blank control[C]		-	1	1	-

[A] All experiments were carried out using two murine CRC cell lines, respectively.

[B] For negative controls, 50μL DPBS without cells were injected

[C] For the blank control, no intervention was performed.

2.6 Anesthesia

Medetomidine (0.5mg/kg, Zoetis, Berlin, Germany), midazolam (5mg/kg, rationpharm GmbH, Ulm, Germany) and fentanyl (0.05mg/kg, Albrecht GmbH, Aulendorf, Germany) were mixed in one syringe (total volume: 2.5mL/kg) and administered via intraperitoneal injection for anesthesia. Animals were then observed for 3-7min in their home cages to allow time for the animals to calm down in an accustomed environment and the drugs to take effect. The depth of anesthesia was assessed by pinching the animal's toe, if there was no withdraw reflex with toe pinch (stage of surgical tolerance), experiments were performed. Mice were placed on a heated pad (Witte+Sutor GmbH, Murrhardt, Germany) to minimize heat loss caused by anesthesia and ophthalmic ointment (Bepanthen® Augen- und Nasensalbe, Bayer Vital GmbH, Leverkusen, Germany) was applied to prevent corneal dryness and trauma during anesthesia (125).

After completion of interventions, surgery or endoscopy, anesthesia was antagonized by intraperitoneal injection of naloxone (1.2 mg/kg, ratiopharm GmbH, Ulm, Germany), flumazenil (0.5 mg/kg, Inresa Arzneimittel GmbH, Freiburg, Germany) and atipamezole (2.5 mg/kg, Vetoquinol GmbH, Ismaning, Germany) mixed to a volume of 8.5 mL/kg body weight. Subsequently, mice were kept on the heated pad and carefully returned to their home cages until full recovery.

2.7 Colonic injection in the EGM

2.7.1 Murine endoscopy

For murine endoscopy, the Coloview® system (Karl Storz, Tuttlingen, Germany) was used.

In detail, a flexible injection catheter (inside diameter 0.28mm, outside diameter 0.61mm, Smiths Medical International Ltd., Kent, UK, Figure 2B) with a 31G needle (Figure 2B) fixed to the end was introduced into the working channel (Figure 2B) of the sheath. The camera (Figure 2A), air infuser (Figure 2A) and light cable (Figure 2A) were assembled to the telescope. Usually a light intensity of 70% of the maximum was sufficient for endoscopy procedures and in order to avoid bias it was not changed during experiments. The white balance was automatically adjusted by pointing the endoscope directly at a white object (such as a piece of paper) which was at a distance of 3–5mm and the focus was set by rotating the focus ring until the object 3-5cm away is sharp. The valve of the Luer lock adapter (Figure 2B) was adjusted to obtain suitable inflation rate, until a slow constant air flow was observed in water of a Falcon 50mL conical centrifuge tube (Corning Science Mexico, Reynosa, Mexico).

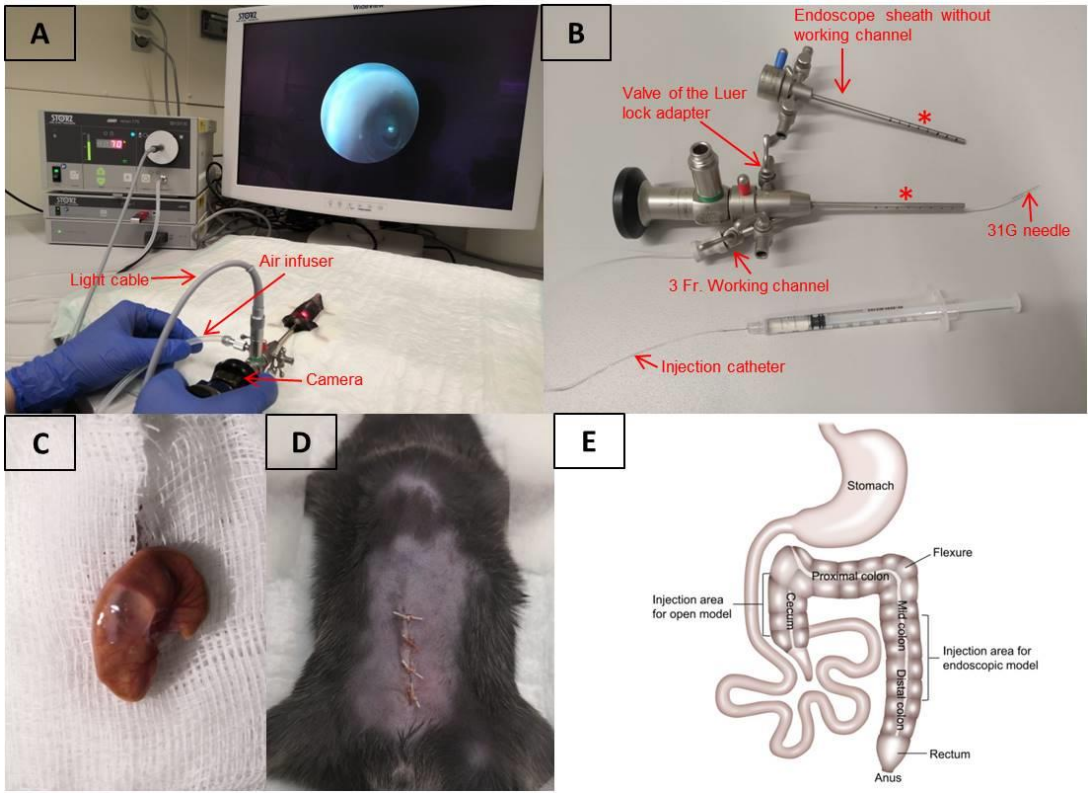

Figure 2. Experimental setup of the EGM and OSM.

(A) Overview of the workplace for murine endoscopy. The camera, air infuser and light cable are assembled to the endoscope. (B) For cell injections in the EGM, a flexible injection catheter with a 31G needle fixed to the end was introduced into the 3Fr. working channel of the 9Fr. examination sheath via a white rubber cap to avoid air leakage, the valve of the Luer lock adapter was used for inflation adjustment. The injection position and location of each identified tumor were recorded based on the gradations (red asterisk) on the endoscope sheath with / without working channel. In the OSM (C), the cecum was exteriorized following laparotomy and a characteristic lifting sign indicated successfully injection. The abdominal wall was finally closed using 4-0 absorbable sutures (D). (E) Murine anatomy of the gastrointestinal tract (126) showing the injection sites of the orthotopic models used in the current study.

The anesthetized mouse was positioned supine on the heated pad and immobilized by adhesive tape. Warm DPBS (1-2mL) was gently applied via a transfer pipette (nerbe plus GmbH & Co. KG, Winsen/Luhe, Germany) to wash the colon (127). As the scope was gently introduced into the colon, the abdomen was carefully monitored to avoid over-inflation since the insufflated intestine could be seen clearly from outside and to localize the tip of the scope with transillumination to avoid over-insertion of the scope. Colonic mucosa was thoroughly examined during colonoscopy to ensure its health prior to cell implantation.

2.7.2 Endoscopy-guided cell implantation

For tumor cell injection, the colonic mucosa was gently penetrated by a 31G needle, with its bevel directed towards the lumen, then 50µL single tumor cell suspension was injected slowly using the Omnican® F syringe (B. Braun Melsungen AG, Hessen, Germany) attached to the other side of the catheter. Blood vessels were carefully avoided when choosing the injection site, since tumor cells injected into a blood vessel or near a damaged blood vessel could cause intravascular dissemination thus distant metastasis. A characteristic lifting sign (128) of the mucosa during injection indicated successful implantation, the needle was withdrawn 10s after injection to make sure that all cells were injected inside. If the initial submucosal injection failed, another three attempts were allowed to undertake. The first attempt should be more proximal, then the needle could be moved distally for further attempts (118, 119). For negative controls, DPBS were injected or no laparotomy was applied. Three different cell concentrations (10^4, 10^5 or 10^6 cells per

50µL injection volume) and four different observation periods (7d, 14d, 21d, 28d) were chosen. The injection position was recorded based on the extent to which the endoscope was inserted by using gradations on the endoscope sheath with working channel (Figure 2B). The endoscope and the 31G needle were disinfected using gigasept® AF forte (2% v/v, Schülke & Mayr GmbH, Norderstedt, Deutschland) followed by water rinse each time before and after use.

After tumor cell implantation, the animals' pain, harm or suffering were assessed everyday according to the standardized score sheet (Table 2) until the end of the experiment. Analgesics (Rimadyl, Zoetis Deutschland GmbH, Berlin, Germany, 5 mg/kg) were injected subcutaneously under any of the following circumstances: repeatedly lick / bite / scratch a particular body part is observed; automutilation; curved back; raised abdomen; visible pedicle.

Table 2**.** Score sheet of systematic assessment for well-being of mice approved by the animal care committee for this study.

Parameter		Evaluation criteria	Score
Outer appearance	☐	Soft and shiny fur, clean body orifices, clear and bright eyes	0
	☐	Fur loss, slight piloerection, slightly unkempt coat, unkempt body orifices, cloudy eyes	5
	☐	Marked / prolonged piloerection, sticky / damp body orifices, abnormal posture / gait	10
	☐	Cramps, paralysis, dyspnea	20
Behavior	☐	Normal behavior	0
	☐	Reduced activity, hyperactivity	10
	☐	Reduced interaction with other mice, reduced food intake, lethargy, pronounced hyperactivity, painful on handling, aggression	20
Body weight	☐	Unaffected: vertebral body and pelvic bone not visible from outside, but palpable by slight pressure[A]	0
	☐	Weight loss < 10%, vertebrae and pelvic bone are discreetly visible and palpable without pressure	5
	☐	Weight loss = 10-19%, skeletal structure is clearly visible[B]	10
	☐	Weight loss > 19%, skeletal structure and intervertebral spaces are clearly visible[C]	20
	☐	Significant weight gain with ascites and / or ileus[D]	20
Clinical findings	☐	Normal	0
	☐	Hypothermia or elevated temperature (< 2°C deviation from normal temperature), dyspnea, palpable tumors present (diameter < 1.5cm)	10
	☐	Severe hypothermia / fever (> 2°C deviation from normal temperature), tachypnoea, diameter of a palpable tumor > 1.5cm	20
Outcome and measures			Total score
	☐	Load level 0	0
	☐	Load level 1 = low load, daily check is required	1-10
	☐	Load level 2 = moderate load, consultation with veterinarians	11-19
	☐	Load level 3 = high-grade load, humane endpoints	> 20

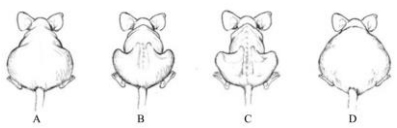

2.7.3 Follow-up colonoscopy

Tumorigenesis in mice of the EGM groups was monitored weekly by follow-up colonoscopy under anesthesia using the same endoscopic system. The average length of insertion was 4cm. Further introduction of the endoscope was limited by the colon's sharp angle at the splenic flexure (Figure 2E). Comparable to human endoscopy, the endoscope was gently inserted and subsequently gradually withdrawn over time. The position (distance from anal verge) of each identified tumor was recorded based on the gradations on the endoscope sheath without working channel (Figure 2B). For semi-quantitative tumor assessment, the Becker scoring system (107) was used: tumor just detectable (score 1), tumor's size / diameter = 1/8 of the lumen diameter (score 2), 1/4 (score 3), 1/2 (score 4) or > 1/2 of the diameter (score 5). Changes in the transparency of the colon, mucosal bleeding, focal lesions as shown in Table 3 were also recorded.

Table 3**.** Follow-up colonoscopy evaluation of mice in the EGM groups.

Wall transparency	☐	Normal
	☐	Most small vessels are invisible
	☐	Only large vessels are visible
	☐	Most blood vessels are invisible
Mucosal bleeding	☐	No bleeding.
	☐	Slightly bleeding
	☐	Significantly bleeding
Focal lesions	☐	Normal, no focal lesions
	☐	Redness or erosion
	☐	Ulceration or stricture
Tumor scoring[A]		1
		2
		3
		4
		5

[A] The tumor was scored according to the Becker scoring system (107)

2.8 Cecal wall injection in the OSM

The animal's lower abdomen was shaved with an electric shaver (Aesculap Suhl GmbH, Suhl, Germany) under anesthesia. The mouse was strapped to the heating pad as described above and laparotomy was performed. Briefly, a small nick (1mm) was made in the skin, through which the abdominal musculature was grasped and lifted up, then the abdominal cavity was entered to extend the incision to 1-2cm using a small scissor. The cecum was exteriorized following laparotomy using sterile pre-cut gauze (Figure 2C) and warm normal saline solution (Fresenius Kabi Deutschland GmbH, Bad Homburg, Germany) was used to keep the cecum always moist. The cecum was gently smoothened by atraumatic forceps. For subserosal injection, a 0.3mL insulin syringe with a 31G needle attached (Becton, Dickinson and Company, NJ, USA) was used. Under a surgical microscope (Zeiss Stemi DV4 SPOT, Carl Zeiss, Göttingen, Germany), cell suspension was injected slowly in the submucosal space. The submucosally placed needle could be visually identified underneath the thin translucent membrane and at the same time above blood vessels. Blood vessels were carefully avoided when choosing the injection site, since tumor cells injected into a blood vessel or near a damaged blood vessel could cause intravascular dissemination thus distant metastasis. A characteristic lifting sign of the serosa during injection indicated successful implantation (Figure 2C). The needle was withdrawn 10s after injection to make sure that all cells were injected inside. If the initial subserosal injection failed, another three attempts were allowed to undertake. Distilled water was then used to thoroughly rinse the cecum with to lyse possibly leaked tumor cells in order to prevent artificial peritoneal tumor cell dissemination. After water rinse, the

cecum was returned back to the abdominal cavity and the abdominal wall was closed with 4-0 absorbable sutures (VICRYLTM Plus, Johnson & Johnson Medical Devices Companies, Diegem, Belgium), specifically, the simple continuous suture was used for peritoneal closure and the simple interrupted suture was used for skin closure (Figure 2D). The povidone iodine (MUNDIPHARMA GmbH, Frankfurt am Main) was applied to the surgical area both before and after laparotomy. For negative controls, DPBS was injected or no laparotomy was performed. Three different cell concentrations (10^4, 10^5 or 10^6 cells per 50µL of injection volume) and four different observation periods (7d, 14d, 21d, 28d) were chosen.

After tumor cell implantation, the animals' pain, harm or suffering were assessed everyday according to the standardized score sheet (Table 2) until the end of the experiment. Follow-up colonoscopy was not performed in the OSM group. Rimadyl was injected subcutaneously under any of the following circumstances: repeatedly lick / bite / scratch a particular body part; automutilation; curved back; raised abdomen; visible pedicle.

2.9 Autopsy

A complete autopsy was performed right after sacrifice according to Prof. Treuting's guideline (129). Any tissue showing evidence of neoplasm or other abnormality was sectioned for histological examination, in particular, abnormal livers (livers with decreased volume / harden liver tissues) were collected sectioned carefully in order not to miss hepatic metastasis. The location, number as well as the size of the tumors and metastases were recorded. The tumor volume was determined based on the formula

Volume = (length × width^2)/2, whereas the length was the largest tumor diameter and the width represented the smallest perpendicular tumor diameter (130).

2.10 Histologic analysis

2.10.1 Formalin-fixed and paraffin embedded tissue processing

Immediately after sacrifice, all organs of interest were harvested and fixed for 12-72h depending on the size of the tissue in 4% neutral buffered formaldehyde solution (SAV-Liquid-Production, Flintsbach am Inn, Germany) at room temperature (RT). The samples were then washed under running tap water for 2h and transferred to 70% ethanol and processed by a Leica Dehydrator Tissue Processor TP1020 (Leica Microsystems Ltd., Shanghai, China) according to manufacturer's protocol (Table 4). After dehydration tissues were embedded in paraffin blocks and RT.

Table 4**.** Leica TP1020 tissue processor protocol.

Reagent	Incubation time (min)
70% Ethanol	120
70% Ethanol	120
70% Ethanol	60
96% Ethanol	90
96% Ethanol	90
100% Ethanol	90
100% Ethanol	90
100% Ethanol	90
NeoClear	90
NeoClear	60
Paraffin	180
Paraffin	180

2.10.2 Agar-paraffin double embedding technique

Embedding tissues in agar prior to tissue processing is very beneficial when working with small and friable samples which was performed according to a previous study (131). A 2% agar solution (w/v, BactoTM Agar, Becton, Dickinson and Company, NJ, USA) was prepared in DPBS and incubated in a water bath at 45^{o}C to prevent from solidification. Briefly, tissues were washed with DPBS 3 times (15min each) after formalin fixation. The appropriate sized moulding was filled with 2% agar solution in which the tissue was immediately placed in and orientated correctly. After the agar block became solid, it was detached from the moulding and trimmed as required leaving a 3-5mm width of agar surrounding the tissue.

2.10.3 Hematoxylin and eosin staining

For Hematoxylin and eosin (H&E) staining, 5µm sections were cut with a Leica Microtome RM 2255 (Leica Microsystems Nußloch GmbH, Nußloch, Germany), transferred to a 46°C water bath and fixed on microscope slides (Paul Marienfeld GmbH & Co. KG, Lauda-Königshofen, Germany). The paraffin sections were deparaffinized, stained and dehydrated according to Table 5, and the coverslips were mounted onto the sections with non-aqueous EUKITT® mounting media (ORSAtec GmbH, Bobingen, Germany). The mounted slides were then examined using an Olympus BX40 Clinical Microscope (Olympus Optical Co., Ltd, Tokyo, Japan) after the mounting medium was fully hardened. Image acquisition was conducted with a Carl Zeiss AxioCam MRc5 Microscope CCD Camera (Carl Zeiss, Göttingen, Germany) and Zen 2 lite software.

Table 5. H&E staining protocol.

Reagent	Incubation time
NeoClear	10min
NeoClear	10min
99% Ethanol	5min
99% Ethanol	5min
96% Ethanol	5min
96% Ethanol	5min
70% Ethanol	5min
70% Ethanol	5min
Distilled water	5min
Tap water	2 dips
Filtered Hematoxylin[A]	3min (with gentle shaking)
Acid ethanol[B]	1 dip
Running tap water	5min
Distilled water	2 dips
Eosin stain[C]	30s (with gentle shaking)
Tap water	2 dips
80% Ethanol	1 dip
96% Ethanol	1 dip
99% Ethanol	1 dip
NeoClear	5min
NeoClear	5min

[A] Hematoxylin: Mayer's hemalum solution, Merck KGaA, Darmstadt, Germany

[B] Acid ethanol: 55mL 1% HCl + 95mL 70% Ethanol

[C] Eosin stain: 1% alcoholic Eosin Y solution (w/v, Eosin Y disodium salt, Sigma, Merck KGaA, Darmstadt, Germany; 96% ethanol)

2.10.4 Immunohistochemical staining

Immunohistochemistry (IHC) was performed on paraffin-embedded sections (4µm thick) with the help of Prof. Neumann's lab (Department of Pathology, LMU). To assess CK20 expression, sections were deparaffinized and rehydrated. Heat mediated antigen retrieval was performed in Tris-EDTA (pH 9.0) at 96°C for 20min. Subsequently, the slides were blocked with BLOXALL™ Blocking Solution (Vector Laboratories, CA, USA), 5% horse serum/TBST, and Avidin/Biotn Blocking Solution (Vector Laboratories), respectively, followed by overnight incubation with rabbit anti-mouse CK20 (Anti-Cytokeratin 20 antibody, Abcam, Berlin, Germany; dilution 1:500) at 4°C. The next day, slides were stained with biotinylated horse anti-rabbit IgG (Vector Laboratories) and signals were detected using ABC-AP Reagent and AP Substrate (Vector Laboratories). After hematoxylin counterstaining, the slides were mounted in aqueous mounting medium (Merck, Darmstadt, Germany) and examined using an Olympus BX40 Clinical Microscope (Olympus, Tokyo, Japan). The image acquisition was conducted with the digital camera Leica DMC4500 (Leica, Wetzlar, Germany) and Leica Application Suite X (LAS X) 3.6.0.20104 software.

2.11 Assessment of tumor infiltrating lymphocytes

Tumor infiltrating lymphocytes (TILs) in both EGM and OSM groups were systematically assessed and quantified (132). This was accomplished by two independent observers (Chen Chen and Prof. Jens Neumann) based on H&E slides of tumor tissues containing the invasive tumor margin, and the Olympus BX40 Clinical Microscope (Olympus Optical

Co., Ltd, Tokyo, Japan; Magnification 200X) was used. Both the TIL score (133, 134) and the Roche score (135) were recorded. Discrepancies were resolved by re-check and a subsequent consensus decision. Regarding the TIL score, only areas of tumor stroma were assessed, and the percentage of stromal TILs was classified as: 0-10% = 1, 11-20% = 2, 21-30% = 3, 31-40% = 4, 41-50% = 5 and 51-100% = 6. For the Roche score, lymphocytes located at the tumor invasive margin, tumor stroma and intra-tumor areas were assessed. The immune phenotype was classified as: 1 = immune desert (nearly no lymphocytes are present within the invasive tumor margin), 2 = immune-excluded tumors (lymphocytes are present at the invasive margin and stroma), 3 = inflamed tumors (lymphocytes are also found in the intra-tumor areas).

2.12 Performance parameter of the establishment

The performance data from 116 mice (EGM) and 105 mice (OSM) were divided into groups of 20 mice in chronological order with the last group (> 100) containing 16 mice (EGM) and 5 mice (OSM) and analyzed. Regarding the learning curve analysis, quality indicators such as success rate of submucosal injection into the colorectal wall, subserosal injection into the cecal wall, adverse event rate, and the duration of each procedure were recorded. Successful submucosal / subserosal injection was defined as observation of a positive lifting sign of the mucosa / serosa indicating no transmural / intracecal injection as well as absence of bleeding at the injection site. Adverse events included colon perforation (EGM) which was defined as either colonoscopically detected bowel perforation or pneumoperitoneum which was characterized by rapid abdominal size

gain, and wound dehiscence and abdominal adhesions with bowel obstruction or ischemia (OSM). A performance score was assigned to each mouse based on the total number of injection attempts and a score of 5 indicated failure. The duration of procedure was counted from the time point of anaesthetic injection to the time point of the endoscope removal (EGM) or to the time point of povidone iodine application on the surgical incision (OSM).

2.13 Statistical analysis

All data were expressed as mean and standard deviation (SD) or as numbers and percentages. Categorical data were analyzed using either the Chi-square test or Fisher's exact test. Continuous variables were compared using the student's t-test and one-way ANOVA with the Bonferroni correction applied for multiple comparisons. Correlation was assessed using bivariate correlation. *P* values less than 0.05 were considered statistically significant. The data were analyzed using GraphPad Prism (version 8.4.0, GraphPad, San Diego, CA) and SPSS (version 23.0, SPSS Inc., Chicago, IL).

3. Results

3.1 Performance characteristics

In EGM group, leakage and perforation of the colon were two reasons of injection failure. In OSM group, injection failure was due to leakage and perforation of the blood vessel and the sutures were completely absorbed on day 18 ± 7 (n = 6, x ± s) for C57BL/6J mice, and day 21 ± 7 (n = 3, x ± s) for BALB/c mice.

The performance score, duration of the procedures, and the adverse event rate depending on the number of interventions carried out in both models, respectively, are shown in Figure 3.

Up to 4 attempts were made on each mouse until the injection was successful. Overall, the rate of successful injection was comparable in both models (performance score < 5, 94% vs. 91%, P = 0.461), the mean performance score of the EGM regarding all procedures was significantly lower than that of the OSM (1.79 ± 1.12 vs. 2.25 ± 1.29, P = 0.006). For both models, performance score and the number of interventions carried out so far showed a significant negative correlation, although the correlation was weak (EGM: r = − 0.197, P = 0.006; OSM: r = − 0.157, P = 0.032). After 40 procedures, the performance score of the EGM significantly decreased (Figure 3A; 2.35 ± 1.42 vs. 1.50 ± 0.78, P = 0.001), whereas a decrease in the OSM was observed after 60 procedures (2.50 ± 1.384 vs. 1.91 ± 1.083, P = 0.020).

Overall, the mean duration of EGM procedures was significantly shorter compared to that of the OSM (11.95 ± 5.07 min vs. 33.73 ± 5.24 min, P < 0.001). For both models, the duration of the procedure and level of experience (procedures performed so far) showed a significant negative relation, although the relation was weak (EGM: r = − 0.144, P = 0.028; OSM: r = − 0.184, P = 0.007). After 20 interventions, the duration of EGM procedures significantly dropped (15.00 ± 6.95 min vs. 11.31 ± 4.36 min, P = 0.033), while a significant reduction in the duration of the OSM was observed occurred after 40 procedures (35.20 ± 5.10 min vs. 32.83 ± 5.17 min, P = 0.024), however, two long procedures were recorded in block 61-80 due to collapsed cecum, which was often difficult to smoothen for subserosal

injection.

Regarding adverse events, 7 cases were recorded in the EGM due to colon perforation, 10 cases were recorded in the OSM derived of wound dehiscence (n=2), abdominal adhesions with bowel obstruction / ischemia (n=8). The overall adverse event rate of the EGM was comparable to that of the OSM (6% vs. 10%, $P = 0.169$). In the EGM group, the adverse event rate and experience level of the investigator demonstrated a significant negative relation ($r = -0.237$, $P = 0.002$). In detail, the mean adverse event rate of the first 40 procedures was 17.5%, and was significantly reduced to 0 afterwards ($P < 0.001$). In the OSM group, a significant negative relation was not found between the adverse event rate and the experience level of the investigator. Only the rate of wound dehiscence was significantly reduced to 0 after the first 20 procedures ($P = 0.003$), abdominal adhesions with bowel obstruction / ischemia was independent of technical procedural factors.

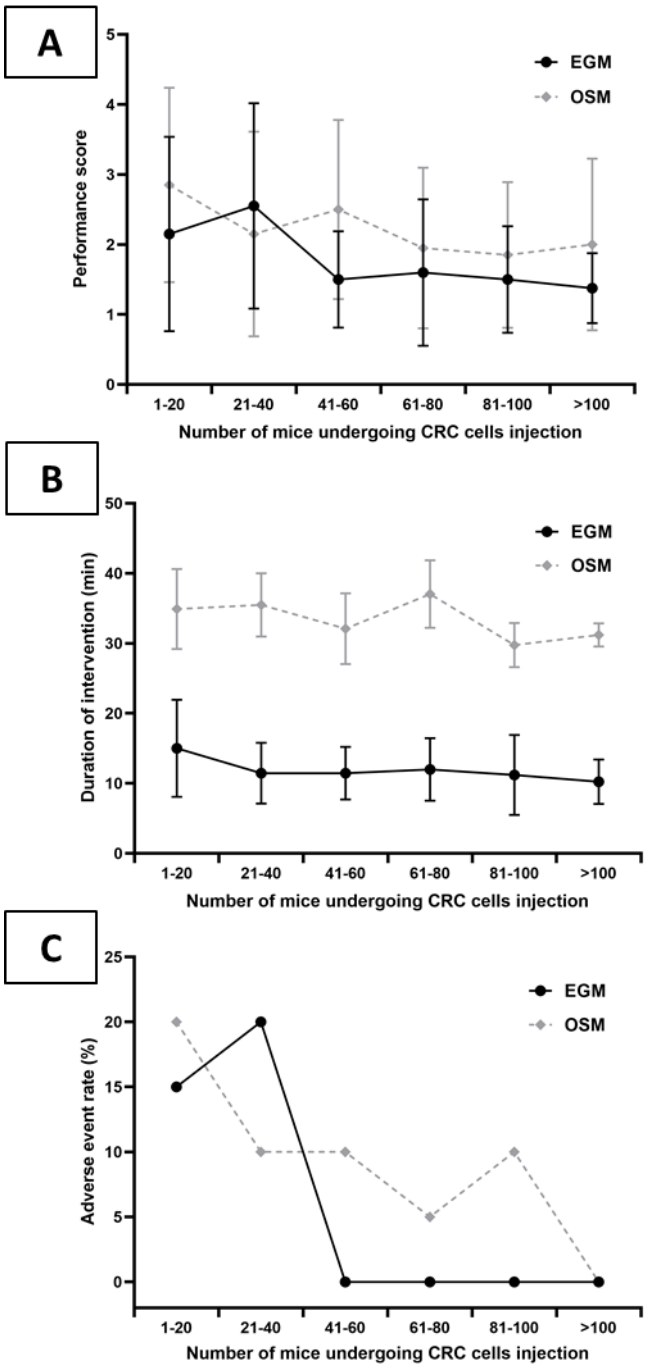

Figure 3**.** Performance characteristics during the establishment process of the EGM and the OSM of CRC.

(A) The mean performance score, (B) the mean duration of an intervention, and (C) the adverse event rate for mice divided into groups of 20 animals with the last group (> 100) containing 16 mice (EGM) and 5 mice (OSM) in chronological order.

3.2 Primary tumor growth

The primary tumor take rate and mortality within the observation period are shown in Tables 6-9 for both cell lines and mouse models, respectively. No gender-dependent differences in primary tumor growth were observed. Representative images from gross examination of mice of both models are shown in Figure 4B-G. The growth kinetics of primary tumors in the EGM group were monitored weekly using the Becker's scoring system and representative colonoscopy images showing endoscopic scores of 3, 4, and 5 are shown in Figure 5B–D. Primary tumor volumes of both models derived from gross autopsy are shown in Figure 5G and H, both cell lines were included. Both macroscopic and microscopic tumor growth were not detected in the negative controls. For the EGM group, the endoscopic scores during follow-up colonoscopy within observation period are demonstrated in Figure 5E. For both cell lines, a significant positive correlation was observed between primary tumor volume and endoscopic score (P = 0.010, Figure 5F).

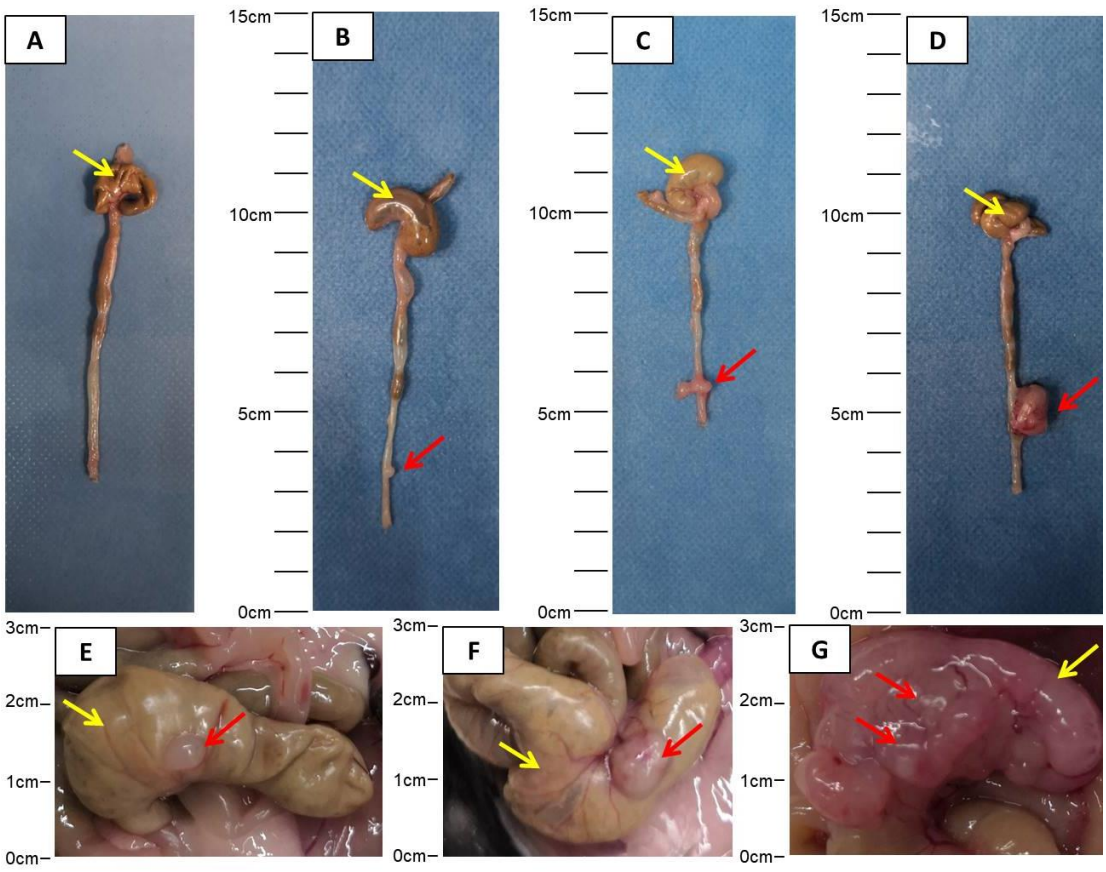

Figure 4**.** Representative images of primary tumors from gross autopsy in both models. (A-D) Representative images of the colorectum (yellow arrows: cecum) of mice in the EGM group showing various sizes of primary tumors in the distal part of the colorectum, and (E-F) the cecum (yellow arrows) of mice in the OSM group showing various sized of primary tumors (red arrows) detected during gross examination.

Table 6**.** Characteristics of the CT26/BALB/c group in the EGM (128).

Number of injected cells	Survival (d)	Mortality [mice(%)]	Tumor take rate [mice(%)]	Tumor volume (mean ± SD, mm^3)	TILs score (mean ± SD)	Metastasis rate[mice(%)][A]		
						Lymph node metastasis	Peritoneal carcinosis	Liver metastasis
10^4	7	0/4 (0)	2/4 (50)	2.5 ± 0.7	3.5 ± 0.7	0/2 (0)	0/2 (0)	0/2 (0)
	14	0/4 (0)	4/4 (100)	2.6 ± 1.5	3.3 ± 1.5	3/4 (75)	0/4 (0)	1/4 (25)
	21	0/4 (0)	4/4 (100)	5.8 ± 2.9	2.5 ± 1.3	1/4 (25)	1/4 (25)	0/4 (0)
	28	0/4 (0)	4/4 (100)	20.0 ± 1.6	2.3 ± 1.3	1/4 (25)	0/4 (0)	0/4 (0)
10^5	7	0/4 (0)	4/4 (100)	4.8 ± 5.2	3.8 ± 1.0	2/4 (50)	0/4 (0)	1/4 (25)
	14	0/4 (0)	4/4 (100)	7.0 ± 7.4	4.5 ± 1.3	4/4 (100)	1/4 (25)	2/4 (50)
	21	0/4 (0)	3/4 (75)	31.0 ± 20.7	3.3 ± 1.5	2/3 (67)	0/3 (0)	0/3 (0)
	28	0/4 (0)	3/4 (75)	22.7 ± 2.3	1.3 ± 0.6	1/3 (33)	0/3 (0)	0/3 (0)
10^6	7	0/4 (0)	4/4 (100)	31.3 ± 17.7	4.3 ± 1.0	2/4 (50)	0/4 (0)	1/4 (25)
	14	0/4 (0)	4/4 (100)	15.8 ± 8.5	2.8 ± 0.5	2/4 (50)	0/4 (0)	2/4 (50)
	21	3/4 (75)[B]	4/4 (100)	44.3 ± 45.2	1.3 ± 0.5	2/4 (50)	0/4 (0)	0/4 (0)
	28	4/4 (100)[B]	4/4 (100)	27.5 ± 11.9	2.3 ± 1.5	2/4 (50)	1/4 (25)	1/4 (25)

[A] Mice with metastasis / mice with primary tumor growth in the group.

[B] The mice were euthanized because of tumor burden.

Table 7**.** Characteristics of the MC38/C57BL/6J group in the EGM (128).

Number of injected cells	Survival (d)	Mortality [mice(%)]	Tumor take rate [mice(%)]	Tumor volume (mean ± SD, mm^3)	TILs score (mean ± SD)	Metastasis rate [mice(%)][A]		
						Lymph node metastasis	Peritoneal carcinosis	Liver metastasis
10^4	7	0/4 (0)	0/4 (0)	-	-	0/0 (0)	0/0 (0)	0/0 (0)
	14	0/4 (0)	0/4 (0)	-	-	0/0 (0)	0/0 (0)	0/0 (0)
	21	0/4 (0)	0/4 (0)	-	-	0/0 (0)	0/0 (0)	0/0 (0)
	28	0/4 (0)	0/4 (0)	-	-	0/0 (0)	0/0 (0)	0/0 (0)
10^5	7	0/4 (0)	0/4 (0)	-	-	0/0 (0)	0/0 (0)	0/0 (0)
	14	0/4 (0)	1/4 (25)	4.0 ± 0.0	1.0 ± 0.0	0/1 (0)	0/1 (0)	0/1 (0)
	21	0/4 (0)	2/4 (50)	2.2 ± 1.3	2.0 ± 1.4	0/2 (0)	0/2 (0)	0/2 (0)
	28	0/4 (0)	3/4 (75)	9.7 ± 5.5	1.7 ± 1.2	2/3 (67)	1/3 (33)	0/3 (0)
10^6	7	0/4 (0)	0/4 (0)	-		0/0 (0)	0/0 (0)	0/0 (0)
	14	0/4 (0)	2/4 (50)	10.0 ± 8.5	1.0 ± 0.0	0/2 (0)	0/2 (0)	0/2 (0)
	21	0/4 (0)	1/4 (25)	18.0 ± 0.0	1.0 ± 0.0	0/1 (0)	0/1 (0)	0/1 (0)
	28	0/4 (0)	2/4 (50)	14.1 ± 15.5	2.0 ± 1.4	1/2 (50)	0/2 (0)	0/2 (0)

[A] Mice with metastasis / mice with primary tumor growth in the group.

Table 8**.** Characteristics of the CT26/BALB/c group in the OSM.

Number of injected cells	Survival (d)	Mortality [mice(%)]	Tumor take rate[mice(%)]	Tumor volume (mean ± SD, mm^3)	TILs score (mean ± SD)	Metastasis rate[mice(%)][A]		
						Lymph node metastasis	Peritoneal carcinosis	Liver metastasis
10^4	7	0/4 (0)	0/4 (0)	-	-	0/0 (0)	0/0 (0)	0/0 (0)
	14	0/4 (0)	3/4 (75)	2.8 ± 2.8	1.0 ± 0.0	1/3 (33)	0/3 (0)	0/3 (0)
	21	0/4 (0)	2/4 (50)	17.0 ± 9.9	1.5 ± 0.7	1/2 (50)	0/2 (0)	1/2 (50)
	28	2/4 (50)[B]	4/4 (100)	15.0 ± 8.1	2.0 ± 0.8	2/4 (50)	2/4 (50)	0/4 (0)
10^5	7	0/4 (0)	1/4 (25)	1.51 ± 0.0	1.0 ± 0.0	0/1 (0)	0/1 (0)	0/1 (0)
	14	0/4 (0)	4/4 (100)	3.5 ± 2.1	1.8 ± 0.5	1/4 (25)	0/4 (0)	1/4 (25)
	21	1/4 (25)[B]	4/4 (100)	5.3 ± 7.2	2.3 ± 1.0	1/4 (25)	1/4 (25)	1/4 (25)
	28	4/4 (100)[B]	4/4 (100)	17.9 ± 12.6	2.5 ± 1.0	0/4 (0)	1/4 (25)	0/4 (0)
10^6	7	0/4 (0)	2/4 (50)	7.0 ± 1.4	1.5 ± 0.7	0/2 (0)	0/2 (0)	0/2 (0)
	14	2/4 (50)[B]	4/4 (100)	11.1 ± 10.3	2.3 ± 1.0	1/4 (25)	1/4 (25)	1/4 (25)
	21	3/4 (75)[B]	3/4 (75)	19.6 ± 11.9	2.3 ± 1.5	1/3 (33)	1/3 (33)	1/3 (33)
	28	4/4 (100)[B]	4/4 (100)	41.6 ± 10.1	3.0 ± 1.6	3/4 (75)	1/4 (25)	2/4 (50)

[A] Mice with metastasis / mice with primary tumor growth in the group.

[B] The mice were euthanized because of tumor burden.

Table 9**.** Characteristics of the MC38/C57BL/6J group in the OSM.

Number of injected cells	Survival (d)	Mortality [mice(%)]	Tumor take rate [mice(%)]	Tumor volume (mm^3)	TILs score	Metastasis rate [mice(%)][A]		
						Lymph node metastasis	Peritoneal carcinosis	Liver metastasis
10^4	7	0/4 (0)	0/4 (0)	-	-	0/0 (0)	0/0 (0)	0/0 (0)
	14	0/4 (0)	0/4 (0)	-	-	0/0 (0)	0/0 (0)	0/0 (0)
	21	0/4 (0)	0/4 (0)	-	-	0/0 (0)	0/0 (0)	0/0 (0)
	28	0/4 (0)	0/4 (0)	-	-	0/0 (0)	0/0 (0)	0/0 (0)
10^5	7	0/4 (0)	0/4 (0)	-	-	0/0 (0)	0/0 (0)	0/0 (0)
	14	0/4 (0)	0/4 (0)	-	-	0/0 (0)	0/0 (0)	0/0 (0)
	21	0/4 (0)	0/4 (0)	-	-	0/0 (0)	0/0 (0)	0/0 (0)
	28	0/4 (0)	1/4 (25)	1.5	3	1/1 (100)	0/1 (0)	0/1 (0)
10^6	7	0/4 (0)	0/4 (0)	-	-	0/0 (0)	0/0 (0)	0/0 (0)
	14	0/4 (0)	0/4 (0)	-	-	0/0 (0)	0/0 (0)	0/0 (0)
	21	0/4 (0)	1/4 (25)	1.0	4	0/1 (0)	1/1 (100)	0/1 (0)
	28	0/4 (0)	1/4 (25)	1.5	4	0/1 (0)	0/1 (0)	0/1 (0)

[A] Mice with metastasis / mice with primary tumor growth in the group.

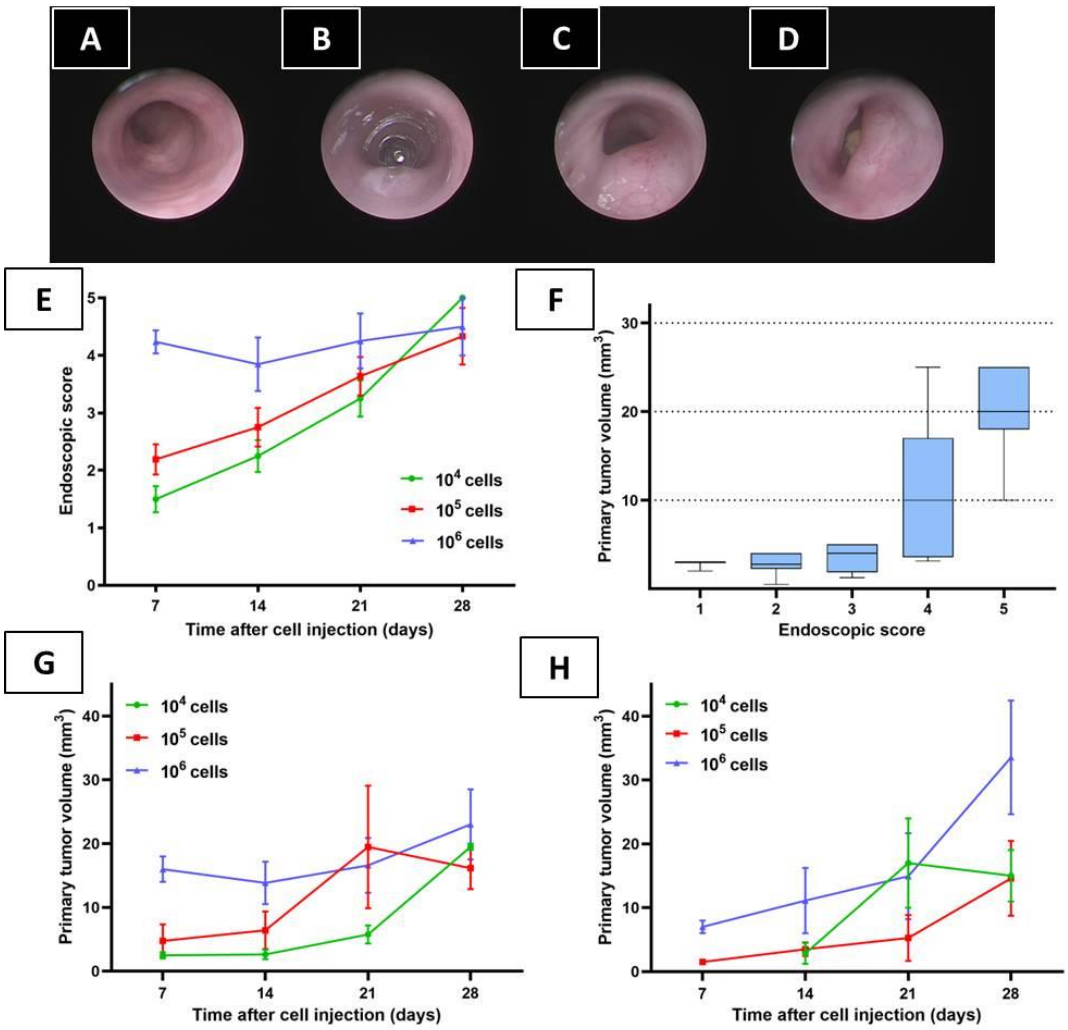

Figure 5**.** Growth kinetics of primary tumors in both EGM and OSM.
(A-D) Representative colonoscopy images in the EGM showing the distal colorectum of (A) a control mouse and different endoscopic scores of tumor growth: (B) score of 3 (~ 1/4 of the lumen), (C) score of 4 (~ 1/2 of the lumen), (D) score of 5 (> 1/2 of the lumen). (E) Endoscopic scores assigned during follow-up colonoscopy to CT26/BALB/c and MC38/C57BL/6J after injection of different numbers of tumor cells, respectively. (F) Box plots of primary tumor volume categorized by the endoscopically assigned score in the EGM group. Mean primary tumor volume derived from both tumor cell lines measured at autopsy (G) in the EGM group and (H) in the OSM group with varying number of implanted cells.

In the MC38/C57BL/6J group, no tumor growth was detected in the 10^4 cell subgroup and at 7 days of observation regardless of the cell number injected, tumors in the EGM were significantly larger than in the OSM (9.4 ± 7.9 mm^3 vs. 1.3 ± 0.3 mm^3, $P = 0.007$). In the CT26/BALB/c group, the same trend was observed, but the difference was not significant ($P = 0.298$).

Regarding the EGM, a significant positive correlation was revealed between tumor volume and observation period ($r = 0.342$, $P = 0.001$) as well as the number of injected cells ($r = 0.38$, $P < 0.001$). The injection of high cell numbers (10^6) led to significantly larger tumors as compared to injection of 10^4 cells (25.8 ± 23.2 mm^3 vs. 7.9 ± 7.9 mm^3, $P = 0.008$) and 10^5 cells (25.8 ± 23.2 mm^3 vs. 12.2 ± 12.9 mm^3, $P = 0.038$), respectively. In addition, tumorigenicity of CT26/BALB/c group was significantly higher than MC38/C57BL/6J group (0.9 ± 0.2 vs. 0.2 ± 0.3, $P < 0.001$). In the OSM, a positive correlation between tumor volume and duration of the observation period was observed ($r = 0.399$, $P < 0.001$). Tumors in the OSM from the 28 days group were significantly larger than the 7 days group (20.1 ± 17.0 mm^3 vs. 2.2 ± 3.4 mm^3, $P = 0.007$) and the 14 days group (20.1 ± 17.0 mm^3 vs. 4.8 ± 6.8 mm^3, $P = 0.027$), respectively. A significant positive correlation was also demonstrated between mortality and duration of the observation period ($r = 0.408$, $P = 0.025$). In OSM group, Compared to the MC38/C57BL/6J, CT26/BALB/c group developed significantly larger tumors (14.1 ± 13.8 mm^3 vs. 1.3 ± 0.3 mm^3, $P < 0.001$), higher tumor take rate (0.7 ± 0.3 vs. 0.1 ± 0.1, $P < 0.001$), and the mortality of CT26/BALB/c was 0.3 ± 0.4, while it was 0 in the MC38/C57BL/6J group.

3.3 Lymph node and distant metastasis

The rate of both, lymph node and distant metastasis, is shown in Tables 6-9 for both models and cell lines, respectively, no further metastasis was observed, such as pulmonary metastasis or cerebral metastasis. No metastatic growth was found in negative controls and animals without primary tumor growth. No gender-dependent differences in metastasis rates were observed. Representative images of gross examination are shown in Figure 6.

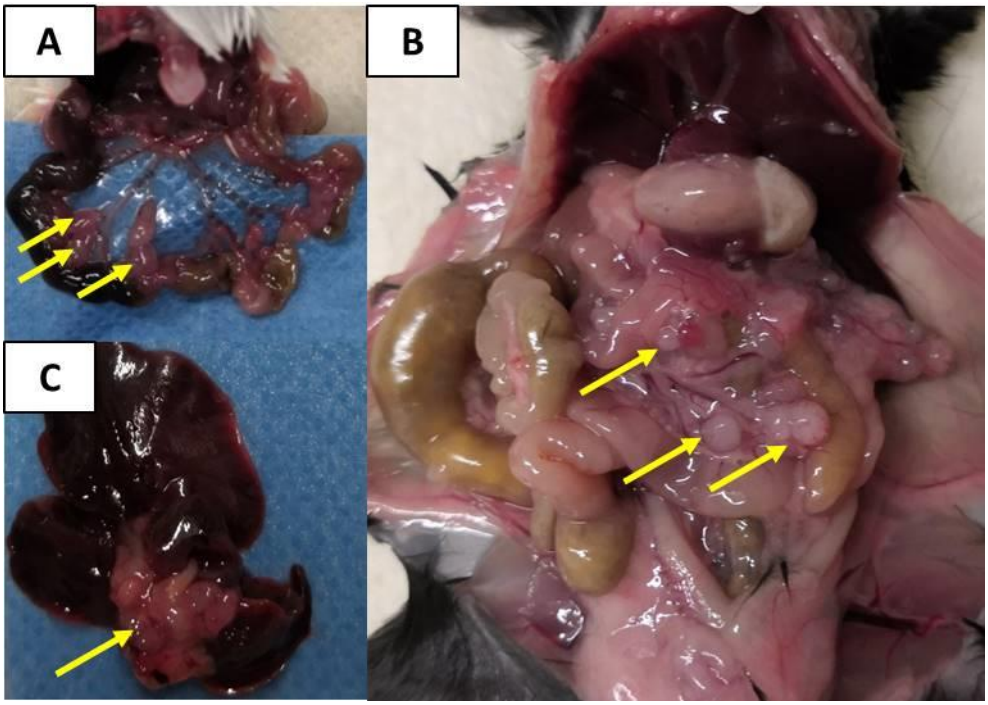

Figure 6**.** Representative images showing metastasis detected during gross examination in EGM (128).
(A) Lymph node metastasis in 10^5 CT26/BALB/c group, (B) peritoneal carcinosis in 10^5 MC38/C57BL/6J group and (C) liver metastasis in 10^5 CT26/BALB/c group. All macroscopic lesions were histologically confirmed.

In EGM, there was a trend regarding negative correlation between metastasis rate and the observation time (r = -0.002, P = 0.985), in addition, a trend towards a positive correlation was seen between metastasis rate and the injected cell number (r = 0.114, P = 0.363). The CT26/BALB/c group revealed a significantly higher overall metastasis rate compared to the MC38/C57BL/6J group (0.2 ± 0.3 vs. 0.1 ± 0.2, P = 0.035). In CT26/BALB/c group, lymph node metastases were only absent from the subgroup of 10^4 cells and the subgroup of 7 days observation; peritoneal carcinosis was found in 3 animals of the CT26/BALB/c group; hepatic metastases were found in 18% animals which developed primary tumors (Table 6). In the MC38/C57BL/6J group, lymph node metastases were only detected in 3 animals on day 28 when more than 10^4 cells were injected (Table 7); peritoneal carcinosis only occurred in one animal; no distant spread was observed.

In the OSM, there was a significant positive relation between metastasis rate and observation time (r = 0.274, P = 0.033), both the 14 days and the 28 days observation groups demonstrated significant higher metastasis rate as compared to that of the 7 days observation group, respectively (0.13 ± 0.14 vs. 0, P = 0.044; 0.26 ± 0.29 vs. 0, P = 0.040). Hepatic metastases were found in 20% mice in CT26/BALB/c group, while none was detected in MC38/C57BL/6J.

3.4 Histology and IHC

Representative H&E as well as IHC staining of primary tumors and metastases are shown in Figures 7 and 8. All EGM derived tumors showed a comparable microscopic malignant phenotype with a moderate atypia of the nuclei. As morphologic characteristics, infiltrating

growth into the colorectal wall and lympho-vascular invasion was noticed (Figure 7A-D). In addition, luminal ulceration of primary tumors was observed frequently. In the OSM, infiltrating growth into the muscularis mucosa was observed (Figure 7E and H).

In the EGM, the TIL score of the CT26/BALB/c group was significantly higher than the MC38/C57BL/6J group across all subgroups (3.0 ± 1.4 vs. 1.5 ± 0.9; $P = 0.003$), while the OSM revealed opposite results (MC38/C57BL/6J vs. CT26/BALB/c = 3.7 ± 0.6 vs. 2.1 ± 1.0; $P = 0.012$). A negative correlation between TILs-score and general metastasis was observed in the OSM ($r = -0.331$, $P = 0.028$).

Tumors of both EGM and OSM showed cytoplasmic positivity for CK20 (Figure 7G and H) with concurrent positive staining of the normal epithelium.

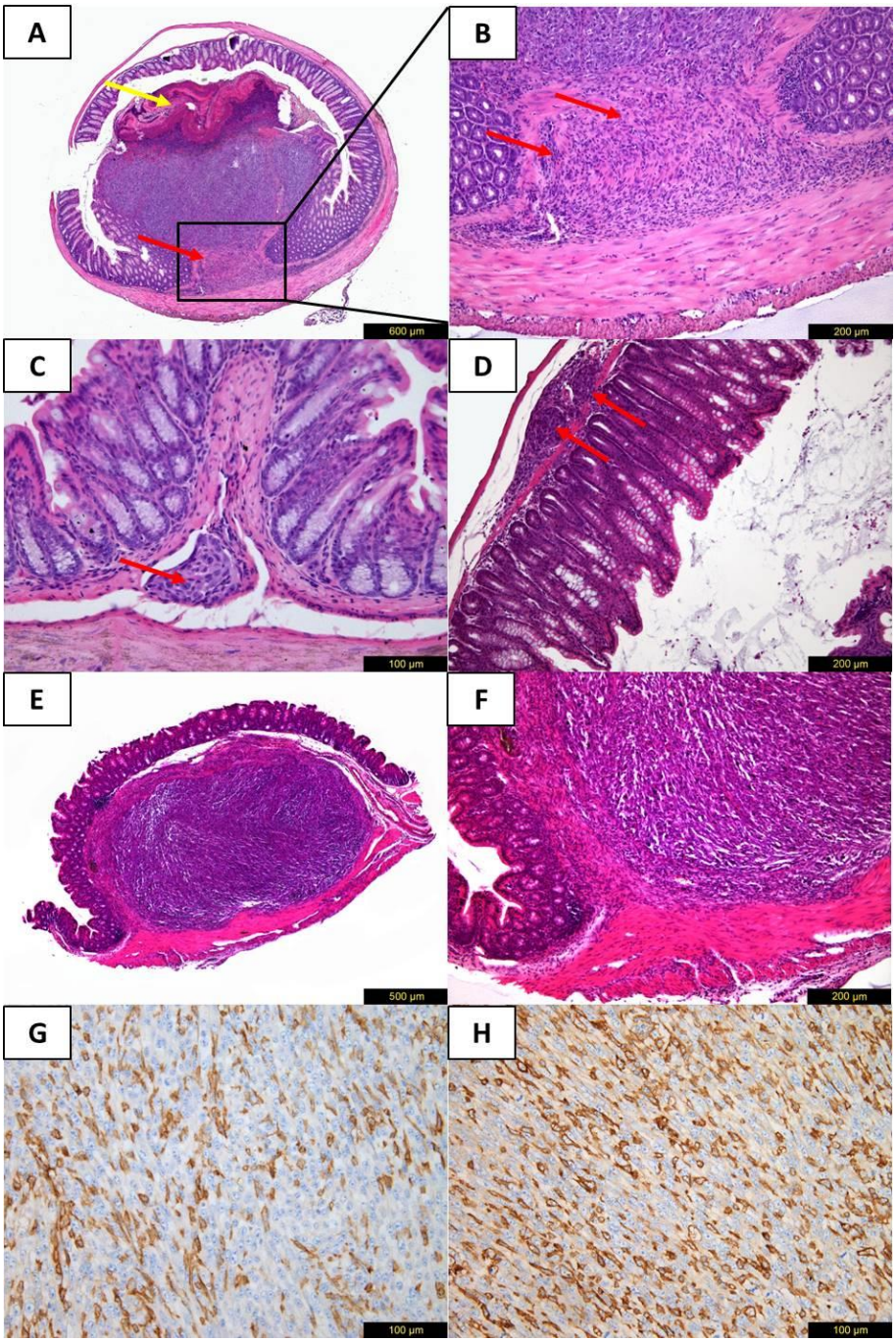

Figure 7**.** H&E and IHC staining of primary tumors in both models.
(A and B) One week after submucosal injection (10^6 CT26 cells) in EGM, the malignant tumor with moderate atypia of the nuclei shows luminal ulceration (A, yellow arrow) and infiltration of the muscularis propria layer (red arrows) corresponding to a pT2-category in humans. (C and D) Representative images of the lympho-vascular invasion (red arrow) in EGM corresponding to a L1-category in humans near primary tumor site. (E and F) One week after subserosal injection (10^6 CT26 cells) in OSM, the tumor cells located in the space between the muscularis mucosa and the muscularis externa of the cecal wall. (G and H) Representative images of cytoplasmic positivity for CK20 in the (G) EGM and (H) OSM.

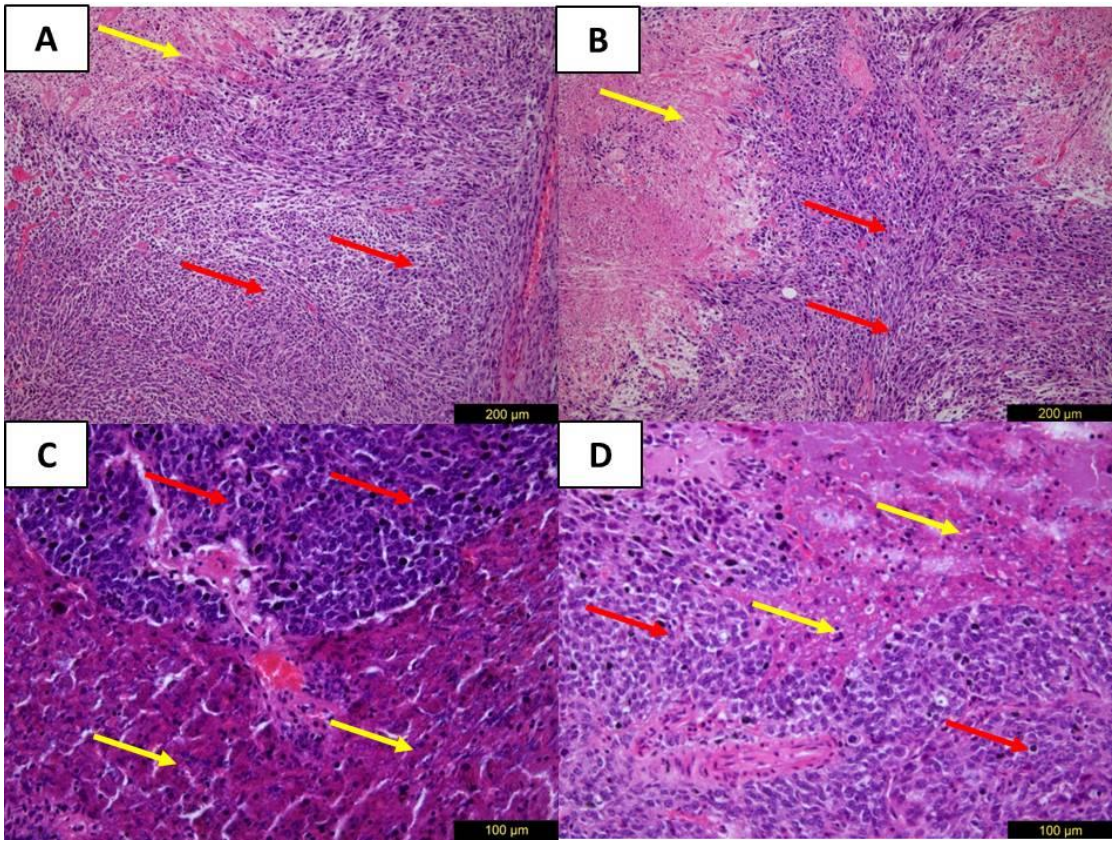

Figure 8**.** H&E staining of metastases in both models.
(A and B) Mesenteric lymph node metastasis with tumor infiltrates (red arrows) and necrosis (yellow arrows) in OSM. (C and D) Hepatic metastasis with tumor infiltrates (red arrows), normal liver tissue (yellow arrows) in EGM.

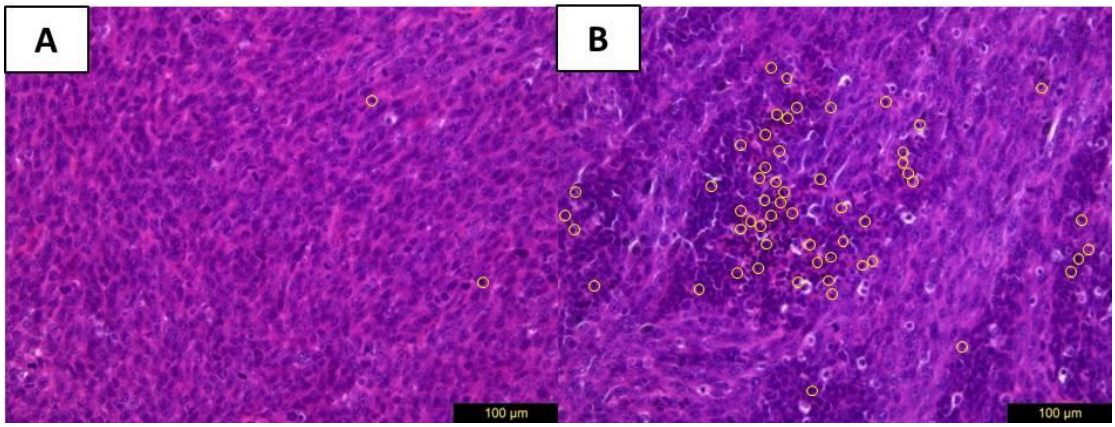

Figure 9**.** Examples of stromal tumor-infiltrating lymphocytes in EGM.
Scoring of stromal tumor-infiltrating lymphocytes (yellow circles) with a score of 1 (0–10% stromal TILs, A) and a score of 6 (>50% stromal TILs, B).

4. Discussion

In the present study, a syngeneic endoscopy-guided minimally invasive orthotopic murine CRC model was established. When compared to the OSM as the gold standard, the EGM was found to be easier to learn, faster to perform, be associated with less complications and more effective regarding local tumor growth with colorectal wall infiltration, luminal ulceration as well as the presence of lympho-vascular invasion. In the current work, the results of two syngeneic approaches (CT26/BALB/c and MC38/C57BL/6J) with application of specific cell concentrations and choosing specific observation periods are shown which could provide guidance for defined experiment settings based on the scientific aim.

The OSM has been the most commonly used method in murine orthotopic CRC implantation models, however this model requires advanced surgical skills and creates surgical traumas (81). Therefore, since endoscopy was first introduced to mice by Alencar *et al.* (82) and Becker *et al.* (106), many attempts have been made in developing EGM which could overcome the drawbacks of OSM. Our study used both CT26/BABL/c and MC38/C57BL/6J syngeneic approaches to establish an EGM.

4.1 Learning curve establishment process

The amount of surgical or technical training required to achieve technical competence for both orthotopic injections models presented in this study is unknown despite increasing demand to train researchers in these procedures. In the medical literature no data on characteristics of such a challenging establishment process is available, however, in

communication with our collaborators, we anecdotally heard of technical difficulties in both models resulting in low research efficacy. Therefore, characterization of the establishment process by assessing parameters of the learning curves was one aim of the present study. Overall, the performance got better as interventions accumulated by time, however, in the OSM group, only the rate of wound dehiscence was significantly reduced to 0 after the first 20 procedures, the abdominal adhesions with bowel obstruction / ischemia may always exist at a rate of 7% regardless of the amount of training, which could have occurred due to bleeding, infection or inflammation. Regarding the technical problems or adverse events in the OSM, related details were only found in two studies. The technical difficulty of the surface injection on cecal wall was mentioned in both studies. In addition, it was observed in one study, that the submucosal injection on the cecal wall could cause early peritoneal carcinosis, which was due to the leaked tumor cell suspension through the tract of the injection needle (84). In the other study, a complication rate of 19.6% was detected during as well as after the procedures, including inflammation of the injection site, leakage of bowel content, and abdominal bleedings (97). The adverse event rate in our EGM was significantly reduced to 0 after the first 40 procedures. Perforation was the only observed adverse event which may be involved in over-inflation and / or intra-luminal injection. Few data are available on complications during murine endoscopy. Zigmond *et al.* reported a complication rate of 5% including perforation and cell leakage to the peritoneal cavity (105). Plummer *et al.* demonstrated 5% perforation rate (136). Those results are in line with ours in the present study (6%).

4.2 Primary tumor growth

In both models, the CT26/BABL/C group showed significantly higher tumor take rates in comparison with the MC38/C57BL/6J group, respectively and more cells were required to initiate tumorigenesis in the MC38/C57BL/6J groups compared to the CT26/BABL/C groups demonstrating the tumorigenesis of CT26 cells to be higher than MC38 cells, which is consistent with previously published studies (117, 137-139). However, the minimal number of cells required for sufficient tumorigenesis varied among studies. Zigmond *et al.* (105) established an EGM within 3 weeks using 10^3 MC38 cells reaching a mean endoscopic score of 3 after 3 weeks; Zhao *et al.* revealed that 10^4 CT26 cells or 10^5 MC38 cells were not enough for primary tumor growth even after 4 weeks of observation (117); Bar-David *et al.* (140) and Rubinstein *et al.* (141) injected 10^4 MC38 cells in another EGM, respectively. Tumors developed after 2 and 4 weeks, respectively. These inconsistence may be explained by variations in the viability of injected tumor cells or even genomic evolution across cell line strains, differences involved in the precision and success of injections (e.g., incorrect injection, trans-mural, intra-luminal), varied host reaction to the cells (142, 143). As for our research, the minimal cell number and observation period to establish a successful EGM were 10^4 CT26 cells at 7 days of observation and 10^5 MC38 cells at 14 days of observation.

4.3 Lymph node and distant metastasis

Regarding distant metastasis in orthotopic models, the reported take rates have been low. In fact, only few orthotopic studies reported spontaneous distant metastasis, and those

rates varied relevantly. Regarding CT26 and MC38 application in OSMs, Tan *et al.* reported 55% hepatic metastasis 10 weeks after MC38 cells injection (72). Kashtan *et al.* found 50% hepatic metastasis 4 weeks following CT26 injection (144), whereas Zhang Y *et al.* revealed 8% hepatic metastasis 8 weeks after CT26 injection (145). Zhang B *et al.* observed 10% hepatic metastasis 5 weeks after CT26 injection (146). Pulmonary metastasis only appeared in immune-deficient mice (69, 83). For CT26 and MC38 application in EGM, Zigmond *et al.* were not able to detect distant spread 3 weeks after cell injection (105). In consistency with these publications, no pulmonary metastasis was found in the present study. In addition, no hepatic metastasis was found in MC38/C57BL/6J group which refers to its lower tumorgenicity regarding local primary tumor growth. In CT26/BALB/c group, the hepatic metastasis rate was 18% in EGM and 20% in OSM, respectively, however, the difference was not significant. When 10^6 CT26 cells were injected, a hepatic metastasis of 25% was able to be achieved in the EGM animals. The shortest observation period with detection of metastasis was only one week, whereas it was two weeks in the OSM. We also observed early development of distant metastasis in up to 50% of mice on day 14 when more than 10^4 CT26 was injected. The differences mentioned above suggest that CT26 cells show higher metastatic potential than MC38 cells. Although this difference was not reported by previous studies, some evidence exists indicating CT26's high invasiveness as well as MC38's rather poor invasiveness (139, 147). It should be noted that some liver metastasis were macroscopically evident as gray nodules on the liver surface whereas others were only visible and confirmed on serial histological sections. In this regard, radiological methods

such as positron emission tomography–computed tomography (PET-CT) or small animal magnetic resonance imaging (MRI) were shown to improve detection of metastasis, however, these techniques are complex and expensive (148-155).

4.4 Assessment of TILs

In the present study, assessment of TILs was performed for the first time in a murine CRC model. This may provide a foundation to use this syngeneic model for translational research regarding the interaction of the tumor and the immune system, e.g. therapy with checkpoint blockade. Our OSM showed a negative correlation between TILs score and metastasis demonstrating that TILs were more prominent in the early stages and decrease in the advanced stages. This is consistent with most cases in humans suggesting that TILs are an indicator for a better prognosis in CRC (134, 156). Furthermore, in the OSM presented in our study, it was revealed that the MC38/C57BL/6J group got significantly higher TILs scores than the CT26/BALB/c group, which may suggest a stronger antitumor immune response involved in the MC38/C57BL/6J group. This may also be part of the explanation why more MC38 cells were needed for sufficient tumorigenesis. On the other hand, the CT26/BALB/c group was scored significantly higher in the EGM. This discrepancy may be due to differences in the surgical trauma and the injection sites. Different microenvironment could lead to different immune profiles and responses to the same cell line. Of note, TILs score itself may not be sufficient to fully describe the organization and distribution of immune response. Further features such as the organization into tertiary lymphoid structures and the presence of hotspots combined

could provide a more precise picture of immune response (134).

4.5 Technical aspects

Although the present EGM is effective regarding tumor growth, some considerations should be kept in mind.

Mice should be at least 10 weeks old thus to enable endoscope introduction without harming the animals. It should be noted that although two operators were optimal for the procedure, one operator was also able to perform the procedure alone after practice.

As for injection needles, researchers picked different sizes ranging from 25G to 33G. To establish a standard procedure of tumor cell implantation in the mouse colon wall, we used 31G needle (Figure 2B). On one hand, its small diameter was observed to reduce the risk of perforation and avoid pneumoperitoneum even in the case of perforation, in addition, it also made slow and gentle injection possible, which helped to cause less harm to murine colon. On the other hand, it provided the rigidity needed for insertion and stability for injection.

The flexible catheter (Figure 2B) attached to the needle was chosen after several tests, optimal wall thickness was evaluated on two aspects, on one hand, it was wide enough to carry the needle, on the other hand, it could roll within the sheath which facilitated the adjustment of needle bevel orientation in the colon.

During colonoscopy, the endoscopic view could be obstructed by feces even after fasting (Figure 10A). Usually feces were moved proximally with gentle air inflation (Figure 10B), if not, 1 mL warm DPBS was applied to wash the colon. DPBS suited well lubricating the

endoscope to facilitate insertion. More than 2 mL DPBS led to blurry / bubble-filled view and this was associated with a higher risk of perforation. Tap water was avoided to clean the colorectum as the mucosa would become less transparent or even white.

High air flow could harm the animal by over inflating the bowel, if the air flow was too low, the mucosa layer would get folded which makes a clear 360 degree view during cell injection impossible. Sometimes the mucosa got folded due to peristalsis (Figure 10C). Hence, it is important to consider that this is not due to a low air flow as only a few seconds are needed in this case for the peristaltic wave to pass (Figure 10D).

The endoscopic score showed a positive correlation with primary tumor volume measured at autopsy, although no linear correlation was observed, colonoscopy is still a good non-invasive tool which can be used for early detection of obstruction or impending obstruction. Two mice reached score 3 and 4 at the second week and stayed alive in good condition with the same endoscopic score until the end of the observation, respectively. One possible reason was that these tumors invaded the submucosa and expanded excentrically towards the serosa (117). Therefore, wall transparency, mucosal bleeding and focal lesions should be considered together with the endoscopic score during follow-up colonoscopy. In addition, imaging of colonoscopy will be complicated around the tumor (endoscopic score ≥ 4) sites by restriction of the colorectal lumen. Hence, suitable time points of follow-up colonoscopy should be chosen if the EGM is used for antitumor treatment.

Based on the great works of Becker *et al.* (107) and Kodani *et al.* (127), the valuable advices from pioneers and experts in the field of murine colonoscopy, Prof. Christoph

Becker and his team, Dr. Chen Varol and Frank Hipp, a checklist with practical tips for the establishment of this model is presented in Table 10 (128).

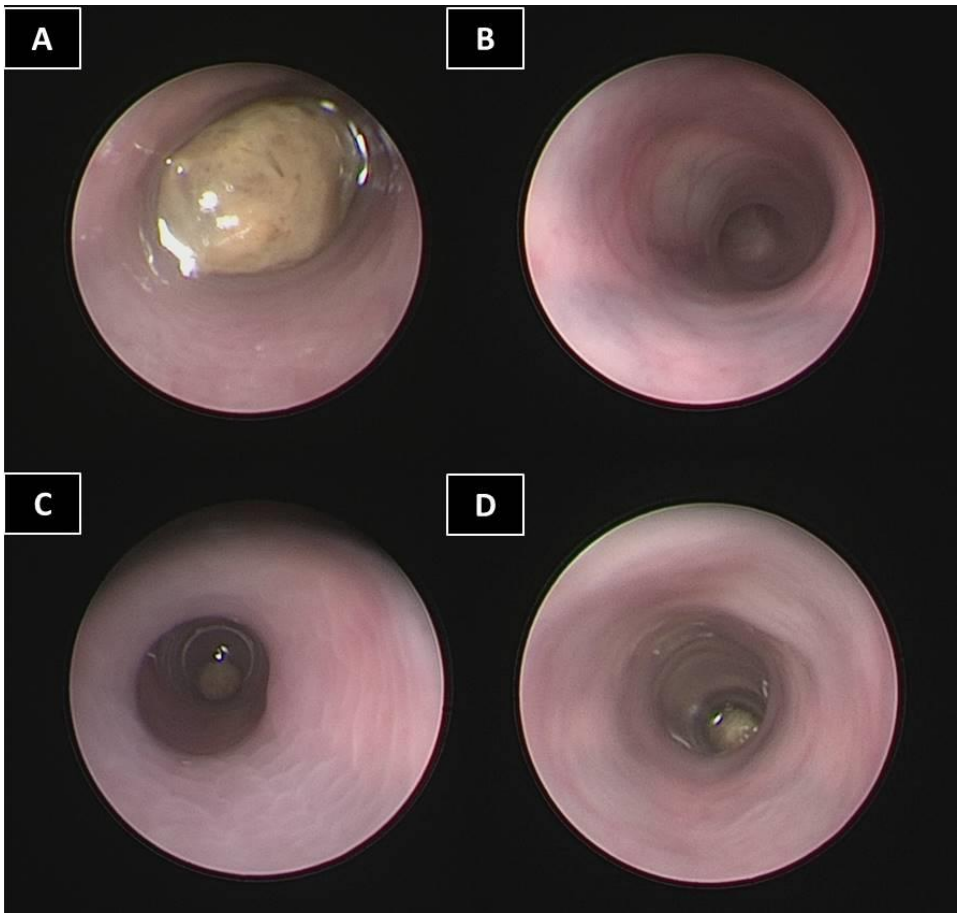

Figure 10**.** Troubleshooting.
If (A) feces obstructed the view, gentle air inflation or DPBS wash can be used for (B) better visibility. If (C) peristaltic movements are observed, wait till the wave pass through (D) without air inflation / scope push.

Figure 11. Checklist of steps and tips for successful establishment of EGM (128).

4.6 Limitations

However, there are some potential limitations of the present study.

Our study was limited to a syngeneic setting as only immune competent mice with injection of the respective murine cell lines were used. Although this kind of approach enables the assessment of the immune system such as TILs, human tumor xenograft studies in immune-deficient mice is still helpful, since cell lines / tumor tissues derived from CRC patients could mimic human CRC process more closely (143).

Only basic functions of the colonoscopy were involved in our EGM, some add ons such as crypt pattern analysis using dye-aided colonoscopy which permits the discrimination between inflammatory and neoplastic changes, fluorescence colonoscopy which can be applied to better locate and visualize tumor growth were not included (107, 118).

In our EGM, metastases were only analyzed during autopsy. BLI, PET-CT and small animal MRI were not used which can detect metastasis development in living mice (152, 157).

5. Conclusion

In conclusion, we successfully established two syngeneic endoscopy-based CRC models and observed some advantages over the OSM as the current gold standard. The results presented in the current study could be used as a guideline for researches that are interested in the establishment of a syngeneic orthotopic mouse model for CRC research that overcomes some of the disadvantages of the OSM. Furthermore, the EGM provides

new possibilities such as minimally invasive follow-up endoscopies including tumor biopsy without the need for sacrificing the animals as well as new visualization techniques. Our results provide the researcher with details regarding the selection of cell line, cell number and observation period for specific research approaches.

6. References

1. Bray F, Ferlay J, Soerjomataram I, Siegel RL, Torre LA, Jemal A. Global cancer statistics 2018: GLOBOCAN estimates of incidence and mortality worldwide for 36 cancers in 185 countries. CA: a cancer journal for clinicians. 2018;68(6):394-424.

2. Bishehsari F, Mahdavinia M, Vacca M, Malekzadeh R, Mariani-Costantini R. Epidemiological transition of colorectal cancer in developing countries: environmental factors, molecular pathways, and opportunities for prevention. World journal of gastroenterology. 2014;20(20):6055-72.

3. Jiang Y, Ben Q, Shen H, Lu W, Zhang Y, Zhu J. Diabetes mellitus and incidence and mortality of colorectal cancer: a systematic review and meta-analysis of cohort studies. European journal of epidemiology. 2011;26(11):863-76.

4. Ma Y, Yang Y, Wang F, Zhang P, Shi C, Zou Y, et al. Obesity and risk of colorectal cancer: a systematic review of prospective studies. PloS one. 2013;8(1):e53916.

5. Chan DS, Lau R, Aune D, Vieira R, Greenwood DC, Kampman E, et al. Red and processed meat and colorectal cancer incidence: meta-analysis of prospective studies. PloS one. 2011;6(6):e20456.

6. Fedirko V, Tramacere I, Bagnardi V, Rota M, Scotti L, Islami F, et al. Alcohol drinking

and colorectal cancer risk: an overall and dose-response meta-analysis of published studies. Annals of oncology : official journal of the European Society for Medical Oncology. 2011;22(9):1958-72.

7. Liang PS, Chen TY, Giovannucci E. Cigarette smoking and colorectal cancer incidence and mortality: systematic review and meta-analysis. International journal of cancer. 2009;124(10):2406-15.

8. Jess T, Rungoe C, Peyrin-Biroulet L. Risk of colorectal cancer in patients with ulcerative colitis: a meta-analysis of population-based cohort studies. Clinical gastroenterology and hepatology : the official clinical practice journal of the American Gastroenterological Association. 2012;10(6):639-45.

9. Eaden JA, Abrams KR, Mayberry JF. The risk of colorectal cancer in ulcerative colitis: a meta-analysis. Gut. 2001;48(4):526-35.

10. von Roon AC, Reese G, Teare J, Constantinides V, Darzi AW, Tekkis PP. The risk of cancer in patients with Crohn's disease. Diseases of the colon and rectum. 2007;50(6):839-55.

11. Cunningham D, Atkin W, Lenz HJ, Lynch HT, Minsky B, Nordlinger B, et al. Colorectal cancer. Lancet (London, England). 2010;375(9719):1030-47.

12. Brenner H, Kloor M, Pox CP. Colorectal cancer. Lancet (London, England). 2014;383(9927):1490-502.

13. Cheng Y, Ling Z, Li L. The Intestinal Microbiota and Colorectal Cancer. Frontiers in immunology. 2020;11:615056.

14. Remo A, Fassan M, Vanoli A, Bonetti LR, Barresi V, Tatangelo F, et al. Morphology

and Molecular Features of Rare Colorectal Carcinoma Histotypes. Cancers. 2019;11(7).

15. Jackman RJ, Mayo CW. The adenoma-carcinoma sequence in cancer of the colon. Surgery, gynecology & obstetrics. 1951;93(3):327-30.

16. Tauriello DV, Calon A, Lonardo E, Batlle E. Determinants of metastatic competency in colorectal cancer. Molecular oncology. 2017;11(1):97-119.

17. Muto T, Bussey HJ, Morson BC. The evolution of cancer of the colon and rectum. Cancer. 1975;36(6):2251-70.

18. Welin S, Youker J, Spratt JS, Jr. The rates and patterns of growth of 375 tumors of the large intestine and rectum observed serially by double contrast enema study (Malmoe technique). The American journal of roentgenology, radium therapy, and nuclear medicine. 1963;90:673-87.

19. Nguyen LH, Goel A, Chung DC. Pathways of Colorectal Carcinogenesis. Gastroenterology. 2020;158(2):291-302.

20. Mármol I, Sánchez-de-Diego C, Pradilla Dieste A, Cerrada E, Rodriguez Yoldi MJ. Colorectal Carcinoma: A General Overview and Future Perspectives in Colorectal Cancer. International journal of molecular sciences. 2017;18(1).

21. Cao H, Xu E, Liu H, Wan L, Lai M. Epithelial-mesenchymal transition in colorectal cancer metastasis: A system review. Pathology, research and practice. 2015;211(8):557-69.

22. Calon A, Espinet E, Palomo-Ponce S, Tauriello DV, Iglesias M, Cespedes MV, et al. Dependency of colorectal cancer on a TGF-beta-driven program in stromal cells for metastasis initiation. Cancer cell. 2012;22(5):571-84.

23. Amin MB, Edge SB. AJCC cancer staging manual: Springer; 2017.

24. Brierley JD, Gospodarowicz MK, Wittekind C. TNM classification of malignant tumours: John Wiley & Sons; 2016.

25. Compton CC. Updated protocol for the examination of specimens from patients with carcinomas of the colon and rectum, excluding carcinoid tumors, lymphomas, sarcomas, and tumors of the vermiform appendix: a basis for checklists. Archives of pathology & laboratory medicine. 2000;124(7):1016-25.

26. J B, M G, C W. International Union Against Cancer: TNM Classification of Malignant Tumours. 8th ed. West Sussex, United Kingdom: Wiley-Blackwell; 2017.

27. CC C, FL G. The Staging of Colorectal Cancer 2004 and Beyond. CA: a cancer journal for clinicians. 2004;54(6):295-308.

28. Boyer B, Thiery JP. Epithelium-mesenchyme interconversion as example of epithelial plasticity. APMIS : acta pathologica, microbiologica, et immunologica Scandinavica. 1993;101(4):257-68.

29. Fidler IJ. The pathogenesis of cancer metastasis: the 'seed and soil' hypothesis revisited. Nature reviews Cancer. 2003;3(6):453-8.

30. Holch JW, Demmer M, Lamersdorf C, Michl M, Schulz C, von Einem JC, et al. Pattern and Dynamics of Distant Metastases in Metastatic Colorectal Cancer. Visceral medicine. 2017;33(1):70-5.

31. Paget S. The distribution of secondary growths in cancer of the breast. Cancer metastasis reviews. 1989;8(2):98-101.

32. RM F-T, AM K, P M, R M, DS I, AC N, et al. Colorectal Cancer: An Update on

Treatment Options and Future Perspectives. Current health sciences journal. 2019;45(2):134-41.

33. Vatandoust S, Price TJ, Karapetis CS. Colorectal cancer: Metastases to a single organ. World journal of gastroenterology. 2015;21(41):11767-76.

34. Johnson RL, Fleet JC. Animal models of colorectal cancer. Cancer metastasis reviews. 2013;32(1-2):39-61.

35. Young M, Ordonez L, Clarke AR. What are the best routes to effectively model human colorectal cancer? Molecular oncology. 2013;7(2):178-89.

36. Vandamme TF. Use of rodents as models of human diseases. Journal of pharmacy & bioallied sciences. 2014;6(1):2-9.

37. Liu E, Kitajima. S, Morimoto. M. Application and recent advances of laboratory mouse in human cancer research. Chinese Journal of Cancer. 2005;24(2):249-54.

38. Treuting PM, Dintzis SM, Montine KS. Comparative anatomy and histology: a mouse, rat, and human atlas: Academic Press; 2017.

39. Krebs C. Experimenteller Alkoholkrebs bei weissen Mäusen. Z Immun Exp Therap. 1928(50):203-18.

40. McIntyre RE, Buczacki SJ, Arends MJ, Adams DJ. Mouse models of colorectal cancer as preclinical models. BioEssays : news and reviews in molecular, cellular and developmental biology. 2015;37(8):909-20.

41. Khanna C, Hunter K. Modeling metastasis in vivo. Carcinogenesis. 2005;26(3):513-23.

42. Hamamoto T, Beppu H, Okada H, Kawabata M, Kitamura T, Miyazono K, et al.

Compound disruption of smad2 accelerates malignant progression of intestinal tumors in apc knockout mice. Cancer research. 2002;62(20):5955-61.

43. Haigis KM, Kendall KR, Wang Y, Cheung A, Haigis MC, Glickman JN, et al. Differential effects of oncogenic K-Ras and N-Ras on proliferation, differentiation and tumor progression in the colon. Nature genetics. 2008;40(5):600-8.

44. Moser AR, Pitot HC, Dove WF. A dominant mutation that predisposes to multiple intestinal neoplasia in the mouse. Science (New York, NY). 1990;247(4940):322-4.

45. Babaei-Jadidi R, Li N, Saadeddin A, Spencer-Dene B, Jandke A, Muhammad B, et al. FBXW7 influences murine intestinal homeostasis and cancer, targeting Notch, Jun, and DEK for degradation. The Journal of experimental medicine. 2011;208(2):295-312.

46. Clarke AR, Cummings MC, Harrison DJ. Interaction between murine germline mutations in p53 and APC predisposes to pancreatic neoplasia but not to increased intestinal malignancy. Oncogene. 1995;11(9):1913-20.

47. Takaku K, Oshima M, Miyoshi H, Matsui M, Seldin MF, Taketo MM. Intestinal tumorigenesis in compound mutant mice of both Dpc4 (Smad4) and Apc genes. Cell. 1998;92(5):645-56.

48. Kucherlapati MH, Lee K, Nguyen AA, Clark AB, Hou H, Jr., Rosulek A, et al. An Msh2 conditional knockout mouse for studying intestinal cancer and testing anticancer agents. Gastroenterology. 2010;138(3):993-1002.e1.

49. Su LK, Kinzler KW, Vogelstein B, Preisinger AC, Moser AR, Luongo C, et al. Multiple intestinal neoplasia caused by a mutation in the murine homolog of the APC gene. Science (New York, NY). 1992;256(5057):668-70.

50. Robanus-Maandag EC, Koelink PJ, Breukel C, Salvatori DC, Jagmohan-Changur SC, Bosch CA, et al. A new conditional Apc-mutant mouse model for colorectal cancer. Carcinogenesis. 2010;31(5):946-52.

51. Shibata H, Toyama K, Shioya H, Ito M, Hirota M, Hasegawa S, et al. Rapid colorectal adenoma formation initiated by conditional targeting of the Apc gene. Science (New York, NY). 1997;278(5335):120-3.

52. Munoz NM, Upton M, Rojas A, Washington MK, Lin L, Chytil A, et al. Transforming growth factor beta receptor type II inactivation induces the malignant transformation of intestinal neoplasms initiated by Apc mutation. Cancer research. 2006;66(20):9837-44.

53. Evans JP, Sutton PA, Winiarski BK, Fenwick SW, Malik HZ, Vimalachandran D, et al. From mice to men: Murine models of colorectal cancer for use in translational research. Critical reviews in oncology/hematology. 2016;98:94-105.

54. Richmond A, Su Y. Mouse xenograft models vs GEM models for human cancer therapeutics. Disease models & mechanisms. 2008;1(2-3):78-82.

55. Gomez-Cuadrado L, Tracey N, Ma R, Qian B, Brunton VG. Mouse models of metastasis: progress and prospects. Disease models & mechanisms. 2017;10(9):1061-74.

56. Pearson HB, Pouliot N. Modeling metastasis in vivo. Madame Curie Bioscience Database [Internet]: Landes Bioscience; 2013.

57. I. C, X. B, M. R, V. M. Characterization of a newly isolated Caco-2 clone (TC7) as a model of transport processes and biotransformation of drugs. Int J Pharm. 1995;116(2):147-58.

58. J. F. Human Tumor Cell In Vitro. New York, USA: Plenum Press; 1975.

59. BH. T, LP. R, MM. J, R. O, CI. K, BD. K. Human colonic adenocarcinoma cells. I. Establishment and description of a new line. In Vitro. 1976;12(3):180-91.

60. A. L, JC. S, 3rd. MW, CE. M, KC. M, ND. M. Classification of human colorectal adenocarcinoma cell lines. Cancer research. 1976;36(12):4562-9.

61. TH. C, Jr. GD, BJ. R, JC. P, Jr. SF. Tumor induction relationships in development of transplantable cancers of the colon in mice for chemotherapy assays, with a note on carcinogen structure. Cancer research. 1975;35(9):2434–9.

62. MG. B, J. S-S, D. F, M. W, AM. S. Establishment of mouse colonic carcinoma cell lines with different metastatic properties. Cancer research. 1980;40(7):2142-6.

63. Golovko D, Kedrin D, Yilmaz Ö H, Roper J. Colorectal cancer models for novel drug discovery. Expert opinion on drug discovery. 2015;10(11):1217-29.

64. M. K-L, I. T, A. D, C. F, MR. H. Review of colorectal cancer and its metastases in rodent models comparative aspects with those in humans. Comp Med. 2000;50(1):16-26.

65. Clevers H. Modeling Development and Disease with Organoids. Cell. 2016;165(7):1586-97.

66. Fatehullah A, Tan SH, Barker N. Organoids as an in vitro model of human development and disease. Nature cell biology. 2016;18(3):246-54.

67. Lancaster MA, Renner M, Martin CA, Wenzel D, Bicknell LS, Hurles ME, et al. Cerebral organoids model human brain development and microcephaly. Nature. 2013;501(7467):373-9.

68. Fumagalli A, Suijkerbuijk SJE, Begthel H, Beerling E, Oost KC, Snippert HJ, et al. A

surgical orthotopic organoid transplantation approach in mice to visualize and study colorectal cancer progression. Nature protocols. 2018;13(2):235-47.

69. Kochall S, Thepkaysone ML, Garcia SA, Betzler AM, Weitz J, Reissfelder C, et al. Isolation of Circulating Tumor Cells in an Orthotopic Mouse Model of Colorectal Cancer. Journal of visualized experiments : JoVE. 2017(125).

70. Karas JR, Essani R, Haughn C, Uchal M, Bishawi MM, Bergamaschi R. Colonoscopic injection for murine solid cecal cancer model. Surgical endoscopy. 2011;25(9):2956-9.

71. MH. G. Murine colon adenocarcinoma: immunobiology of metastases. Cancer. 1980 45(5 Suppl):1223-8.

72. Tan MH, Holyoke ED, Goldrosen MH. Murine colon adenocarcinoma: syngeneic orthotopic transplantation and subsequent hepatic metastases. Journal of the National Cancer Institute. 1977;59(5):1537-44.

73. Bresalier R, Raper S, Hujanen E, Kim Y. A new animal model for human colon cancer metastasis. Int J Cancer. 1987;39(5):625-30.

74. Bresalier RS, Hujanen ES, Raper SE, Roll FJ, Itzkowitz SH, Martin GR, et al. An animal model for colon cancer metastasis: establishment and characterization of murine cell lines with enhanced liver-metastasizing ability. Cancer research. 1987;47(5):1398-406.

75. Goldrosen MH. Murine colon adenocarcinoma: immunobiology of metastases. Cancer. 1980;45(5 Suppl):1223-8.

76. Nakajima M, Morikawa K, Fabra A, Bucana CD, Fidler IJ. Influence of organ environment on extracellular matrix degradative activity and metastasis of human colon

carcinoma cells. Journal of the National Cancer Institute. 1990;82(24):1890-8.

77. Wilmanns C, Fan D, O'Brian CA, Bucana CD, Fidler IJ. Orthotopic and ectopic organ environments differentially influence the sensitivity of murine colon carcinoma cells to doxorubicin and 5-fluorouracil. International journal of cancer. 1992;52(1):98-104.

78. Morikawa K, Walker SM, Nakajima M, Pathak S, Jessup JM, Fidler IJ. Influence of organ environment on the growth, selection, and metastasis of human colon carcinoma cells in nude mice. Cancer research. 1988;48(23):6863-71.

79. Schackert HK, Fidler IJ. Development of an animal model to study the biology of recurrent colorectal cancer originating from mesenteric lymph system metastases. International journal of cancer. 1989;44(1):177-81.

80. Fidler IJ. Orthotopic implantation of human colon carcinomas into nude mice provides a valuable model for the biology and therapy of metastasis. Cancer metastasis reviews. 1991;10(3):229-43.

81. Tseng W, Leong X, Engleman E. Orthotopic mouse model of colorectal cancer. Journal of visualized experiments : JoVE. 2007(10):484.

82. Alencar H, King R, Funovics M, Stout C, Weissleder R, Mahmood U. A novel mouse model for segmental orthotopic colon cancer. International journal of cancer. 2005;117(3):335-9.

83. Cespedes MV, Espina C, Garcia-Cabezas MA, Trias M, Boluda A, Gomez del Pulgar MT, et al. Orthotopic microinjection of human colon cancer cells in nude mice induces tumor foci in all clinically relevant metastatic sites. The American journal of pathology. 2007;170(3):1077-85.

84. Terracina KP, Aoyagi T, Huang WC, Nagahashi M, Yamada A, Aoki K, et al. Development of a metastatic murine colon cancer model. The Journal of surgical research. 2015;199(1):106-14.

85. B. R, R. G, A. S, FX. S, J. G, AR. M, et al. An Orthotopic Mouse Model of Remetastasis of Human Colon Cancer Liver Metastasis. Clinical Cancer Research. 2000;6(6):2556-61.

86. Jin H, Liu X, Li VK, Ding Y, Yun S, Liu F, et al. A simple colostomy implantation model for evaluating colon cancer. International journal of colorectal disease. 2009;24(1):41-7.

87. Seguin J, Doan BT, Latorre Ossa H, Juge L, Gennisson JL, Tanter M, et al. Evaluation of Nonradiative Clinical Imaging Techniques for the Longitudinal Assessment of Tumour Growth in Murine CT26 Colon Carcinoma. International journal of molecular imaging. 2013;2013:983534.

88. Endo T, Toda M, Watanabe M, Iizuka Y, Kubota T, Kitajima M, et al. In situ cancer vaccination with a replication-conditional HSV for the treatment of liver metastasis of colon cancer. Cancer gene therapy. 2002;9(2):142-8.

89. O'Rourke KP, Loizou E, Livshits G, Schatoff EM, Baslan T, Manchado E, et al. Transplantation of engineered organoids enables rapid generation of metastatic mouse models of colorectal cancer. Nature biotechnology. 2017;35(6):577-82.

90. Onuma K, Ochiai M, Orihashi K, Takahashi M, Imai T, Nakagama H, et al. Genetic reconstitution of tumorigenesis in primary intestinal cells. Proceedings of the National Academy of Sciences of the United States of America. 2013;110(27):11127-32.

91. Sun FX, Sasson AR, Jiang P, An Z, Gamagami R, Li L, et al. An ultra-metastatic

model of human colon cancer in nude mice. Clinical & experimental metastasis. 1999;17(1):41-8.

92. Fu XY, Besterman JM, Monosov A, Hoffman RM. Models of human metastatic colon cancer in nude mice orthotopically constructed by using histologically intact patient specimens. Proceedings of the National Academy of Sciences of the United States of America. 1991;88(20):9345-9.

93. Donigan M, Loh BD, Norcross LS, Li S, Williamson PR, DeJesus S, et al. A metastatic colon cancer model using nonoperative transanal rectal injection. Surgical endoscopy. 2010;24(3):642-7.

94. Ahnen DJ, Wade SW, Jones WF, Sifri R, Mendoza Silveiras J, Greenamyer J, et al. The increasing incidence of young-onset colorectal cancer: a call to action. Mayo Clinic proceedings. 2014;89(2):216-24.

95. JS. L, MA. P, LA. P, CM. R, EM. W, E. OC, et al. Screening for Colorectal Cancer: A Systematic Review for the U.S. Preventive Services Task Force. JAMA. 2016;315(23):2576-94.

96. Heijstek MW, Kranenburg O, Borel Rinkes IH. Mouse models of colorectal cancer and liver metastases. Digestive surgery. 2005;22(1-2):16-25.

97. Thiran A. The effect of colorectal surgery on liver metastases. Ghent University. 2019.

98. H. K, M. R, JB. M, AH. W, JC. R, B. S, et al. Intra-rectal injection of tumor cells: a novel animal model of rectal cancer. Surg Oncol. 1992;1(3):251-6.

99. Donigan M, Norcross LS, Aversa J, Colon J, Smith J, Madero-Visbal R, et al. Novel murine model for colon cancer: non-operative trans-anal rectal injection. The Journal of

surgical research. 2009;154(2):299-303.

100.Enquist IB, Good Z, Jubb AM, Fuh G, Wang X, Junttila MR, et al. Lymph node-independent liver metastasis in a model of metastatic colorectal cancer. Nature communications. 2014;5:3530.

101.T. T, M. M, K. N. A novel mouse model of rectal cancer established by orthotopic implantation of colon cancer cells. Cancer Sci. 2004;95(6):514-9.

102.H. K, M. M, R. A, H. K, A. S, M. B, et al. Development of a clinically-precise mouse model of rectal cancer. PloS one. 2013;8(11):e79453.

103.Bhullar JS, Subhas G, Silberberg B, Tilak J, Andrus L, Decker M, et al. A novel nonoperative orthotopic colorectal cancer murine model using electrocoagulation. Journal of the American College of Surgeons. 2011;213(1):54-60; discussion -1.

104.Pox C. Update der S3-Leitlinie zum kolorektalen Karzinom. best practice onkologie. 2018;13(5):254-62.

105.Zigmond E, Halpern Z, Elinav E, Brazowski E, Jung S, Varol C. Utilization of murine colonoscopy for orthotopic implantation of colorectal cancer. PloS one. 2011;6(12):e28858.

106.Becker C, Fantini MC, Wirtz S, Nikolaev A, Kiesslich R, Lehr HA, et al. In vivo imaging of colitis and colon cancer development in mice using high resolution chromoendoscopy. Gut. 2005;54(7):950-4.

107.Becker C, Fantini MC, Neurath MF. High resolution colonoscopy in live mice. Nature protocols. 2006;1(6):2900-4.

108.Neurath MF, Wittkopf N, Wlodarski A, Waldner M, Neufert C, Wirtz S, et al.

Assessment of tumor development and wound healing using endoscopic techniques in mice. Gastroenterology. 2010;139(6):1837-43 e1.

109. Adachi T, Hinoi T, Sasaki Y, Niitsu H, Saito Y, Miguchi M, et al. Colonoscopy as a tool for evaluating colorectal tumor development in a mouse model. International journal of colorectal disease. 2014;29(2):217-23.

110. M. B, P. L, TM. N, F. P, D. F, D. B. Murine endoscopy for in vivo multimodal imaging of carcinogenesis and assessment of intestinal wound healing and inflammation. Journal of visualized experiments : JoVE. 2014;26(90):1-9.

111. Huang EH, Carter JJ, Whelan RL, Liu YH, Rosenberg JO, Rotterdam H, et al. Colonoscopy in Mice. Surgical Endoscopy And Other Interventional Techniques. 2001;16(1):22-4.

112. Wirtz S, Becker C, Blumberg R, Galle PR, Neurath MF. Treatment of T Cell-Dependent Experimental Colitis in SCID Mice by Local Administration of an Adenovirus Expressing IL-18 Antisense mRNA. The Journal of Immunology. 2002;168(1):411-20.

113. Foersch S, Neufert C, Neurath MF, Waldner MJ. Endomicroscopic Imaging of COX-2 Activity in Murine Sporadic and Colitis-Associated Colorectal Cancer. Diagnostic and therapeutic endoscopy. 2013;2013:250641.

114. Mitsunaga M, Kosaka N, Choyke PL, Young MR, Dextras CR, Saud SM, et al. Fluorescence endoscopic detection of murine colitis-associated colon cancer by topically applied enzymatically rapid-activatable probe. Gut. 2013;62(8):1179-86.

115. Martin ES, Belmont PJ, Sinnamon MJ, Richard LG, Yuan J, Coffee EM, et al.

Development of a colon cancer GEMM-derived orthotopic transplant model for drug discovery and validation. Clinical cancer research : an official journal of the American Association for Cancer Research. 2013;19(11):2929-40.

116. Bettenworth D, Mucke MM, Schwegmann K, Faust A, Poremba C, Schafers M, et al. Endoscopy-guided orthotopic implantation of colorectal cancer cells results in metastatic colorectal cancer in mice. Clinical & experimental metastasis. 2016;33(6):551-62.

117. X. Z, L. L, TK. S, S. S. Tumor location impacts immune response in mouse models of colon cancer. Oncotarget. 2017;8(33):54775-87.

118. Roper J, Tammela T, Cetinbas NM, Akkad A, Roghanian A, Rickelt S, et al. In vivo genome editing and organoid transplantation models of colorectal cancer Nature biotechnology. 2017;35(6):569-76.

119. Roper J, Tammela T, Akkad A, Almeqdadi M, Santos SB, Jacks T, et al. Colonoscopy-based colorectal cancer modeling in mice with CRISPR-Cas9 genome editing and organoid transplantation. Nature protocols. 2018;13(2):217-34.

120. Kemeny N. Presurgical chemotherapy in patients being considered for liver resection. The oncologist. 2007;12(7):825-39.

121. Gonzalez M, Poncet A, Combescure C, Robert J, Ris HB, Gervaz P. Risk factors for survival after lung metastasectomy in colorectal cancer patients: a systematic review and meta-analysis. Annals of surgical oncology. 2013;20(2):572-9.

122. Szabo V, Bugyik E, Dezso K, Ecker N, Nagy P, Timar J, et al. Mechanism of tumour vascularization in experimental lung metastases. The Journal of pathology. 2015;235(3):384-96.

123.Guillen J. FELASA guidelines and recommendations. Journal of the American Association for Laboratory Animal Science : JAALAS. 2012;51(3):311-21.

124.Kilkenny C, Browne WJ, Cuthill IC, Emerson M, Altman DG. Improving bioscience research reporting: the ARRIVE guidelines for reporting animal research. Osteoarthritis and cartilage. 2012;20(4):256-60.

125.Adams S, Pacharinsak C. Mouse anesthesia and analgesia. Current protocols in mouse biology. 2015;5(1):51-63.

126.Freeling JL, Rezvani K. Assessment of murine colorectal cancer by micro-ultrasound using three dimensional reconstruction and non-linear contrast imaging. Molecular therapy Methods & clinical development. 2016;5:16070.

127.Kodani T, Rodriguez-Palacios A, Corridoni D, Lopetuso L, Di Martino L, Marks B, et al. Flexible colonoscopy in mice to evaluate the severity of colitis and colorectal tumors using a validated endoscopic scoring system. Journal of visualized experiments : JoVE. 2013(80):e50843.

128.Chen C, Neumann J, Kühn F, Lee SML, Drefs M, Andrassy J, et al. Establishment of an Endoscopy-Guided Minimally Invasive Orthotopic Mouse Model of Colorectal Cancer. Cancers. 2020;12(10).

129.Treuting PM, Snyder JM. Mouse Necropsy. Current protocols in mouse biology. 2015;5(3):223-33.

130.Mirniaharikandehei S, VanOsdol J, Heidari M, Danala G, Sethuraman SN, Ranjan A, et al. Developing a Quantitative Ultrasound Image Feature Analysis Scheme to Assess Tumor Treatment Efficacy Using a Mouse Model. Scientific reports. 2019;9(1):7293.

131. Yadav L, Thomas S, Kini U. Improvised double-embedding technique of minute biopsies: a mega boon to histopathology laboratory. Indian J Pathol Microbiol. 2015;58(1):12-6.

132. Galon J, Lanzi A. Immunoscore and its introduction in clinical practice. The quarterly journal of nuclear medicine and molecular imaging : official publication of the Italian Association of Nuclear Medicine (AIMN) [and] the International Association of Radiopharmacology (IAR), [and] Section of the So. 2020;64(2):152-61.

133. Salgado R, Denkert C, Demaria S, Sirtaine N, Klauschen F, Pruneri G, et al. The evaluation of tumor-infiltrating lymphocytes (TILs) in breast cancer: recommendations by an International TILs Working Group 2014. Annals of oncology : official journal of the European Society for Medical Oncology. 2015;26(2):259-71.

134. Hendry S, Salgado R, Gevaert T, Russell PA, John T, Thapa B, et al. Assessing Tumor-infiltrating Lymphocytes in Solid Tumors: A Practical Review for Pathologists and Proposal for a Standardized Method From the International Immunooncology Biomarkers Working Group: Part 1: Assessing the Host Immune Response, TILs in Invasive Breast Carcinoma and Ductal Carcinoma In Situ, Metastatic Tumor Deposits and Areas for Further Research. Advances in anatomic pathology. 2017;24(5):235-51.

135. Beyond the immunity cycle. Available from: https://www.roche.com/research_and_development/what_we_are_working_on/oncology/cancer-immunotherapy/beyond-the-immunity-cycle.htm.

136. Plummer R, Papageorge M, Ciomek N, Liu T, Yoo J. Myofibroblasts Enhance Tumor Growth in a Novel Mouse Model of Colorectal Cancer. The Journal of surgical research.

2019;244:374-81.

137. Franken NA, Rodermond HM, Stap J, Haveman J, Van Bree C. Clonogenic assay of cells in vitro. Nature protocols. 2006;1(5):2315-9.

138. Liu H, Liu H, Zhou Z, Parise RA, Chu E, Schmitz JC. Herbal formula Huang Qin Ge Gen Tang enhances 5-fluorouracil antitumor activity through modulation of the E2F1/TS pathway. Cell Communication and Signaling. 2018;16(1):1-12.

139. Brattain MG, Strobel-Stevens J, Fine D, Webb M, Sarrif AM. Establishment of mouse colonic carcinoma cell lines with different metastatic properties. Cancer research. 1980;40(7):2142-6.

140. Bar-David S, Larush L, Goder N, Aizic A, Zigmond E, Varol C, et al. Size and lipid modification determine liposomal Indocyanine green performance for tumor imaging in a model of rectal cancer. Scientific reports. 2019;9(1):8566.

141. Arbel Rubinstein T, Shahmoon S, Zigmond E, Etan T, Merenbakh-Lamin K, Pasmanik-Chor M, et al. Klotho suppresses colorectal cancer through modulation of the unfolded protein response. Oncogene. 2019;38(6):794-807.

142. Ben-David U, Siranosian B, Ha G, Tang H, Oren Y, Hinohara K, et al. Genetic and transcriptional evolution alters cancer cell line drug response. Nature. 2018;560(7718):325-30.

143. Oliveira RC, Abrantes AM, Tralhão JG, Botelho MF. The role of mouse models in colorectal cancer research—The need and the importance of the orthotopic models. Animal Models and Experimental Medicine. 2020;3(1):1-8.

144. Kashtan H, Rabau M, Mullen JB, Wong AH, Roder JC, Shpitz B, et al. Intra-rectal

injection of tumour cells: a novel animal model of rectal cancer. Surgical oncology. 1992;1(3):251-6.

145.Zhang Y, Davis C, Ryan J, Janney C, Pena MM. Development and characterization of a reliable mouse model of colorectal cancer metastasis to the liver. Clinical & experimental metastasis. 2013;30(7):903-18.

146.Zhang B, Zhang B, Chen X, Bae S, Singh K, Washington MK, et al. Loss of Smad4 in colorectal cancer induces resistance to 5-fluorouracil through activating Akt pathway. British journal of cancer. 2014;110(4):946-57.

147.Smith JJ, Deane NG, Wu F, Merchant NB, Zhang B, Jiang A, et al. Experimentally derived metastasis gene expression profile predicts recurrence and death in patients with colon cancer. Gastroenterology. 2010;138(3):958-68.

148.Robinson P. The early detection of liver metastases. Cancer Imaging. 2002;2(2):1-3.

149.Lavilla-Alonso S, Abo-Ramadan U, Halavaara J, Escutenaire S, Tatlisumak T, Saksela K, et al. Optimized mouse model for the imaging of tumor metastasis upon experimental therapy. PloS one. 2011;6(11):e26810.

150.Ge Y, Ding Y, Zhang J, Li Z, Li Z. Effect of angiogenesis inhibitor SU6668 in combination with 5-Fu on liver metastasis from transplantation tumors of human colorectal cancer in nude mice. International journal of clinical and experimental medicine. 2014;7(10):3578-82.

151.Kawai K, Tamura K, Sakata I, Ishida J, Nagata M, Tsukada H, et al. A new in vivo model to analyze hepatic metastasis of the human colon cancer cell line HCT116 in NOD/Shi-scid/IL-2Rγ(null) (NOG) mice by (18)F-FDG PET/CT. Oncology reports.

2013;29(2):464-8.

152.Peldschus K, Ittrich H. Magnetic resonance imaging of metastases in xenograft mouse models of cancer. Methods in molecular biology. 2014;1070:213-22.

153.Haldorsen IS, Popa M, Fonnes T, Brekke N, Kopperud R, Visser NC, et al. Multimodal Imaging of Orthotopic Mouse Model of Endometrial Carcinoma. PloS one. 2015;10(8):e0135220.

154.Usuda K, Sagawa M, Motomo N, Ueno M, Tanaka M, Machida Y, et al. Recurrence and Metastasis of Lung Cancer Demonstrate Decreased Diffusion on Diffusion-Weighted Magnetic Resonance Imaging. Asian Pacific Journal of Cancer Prevention. 2014;15(16):6843-8.

155.JS L, S A, JR G, R L, MJ W. Small animal imaging：current technology and perspectives for oncological imaging. European journal of cancer. 2002;38(16):2173-88.

156.Ohtani H. Focus on TILs: prognostic significance of tumor infiltrating lymphocytes in human colorectal cancer. Cancer immunity. 2007;7:4.

157.Lewis JS, Achilefu S, Garbow JR, Laforest R, Welch MJ. Small animal imaging. current technology and perspectives for oncological imaging. European journal of cancer. 2002;38(16):2173-88.

Acknowledgement

I would like to thank…

Prof. Dr. Alexandr Bazhin for giving me the opportunity to carry out my Ph.D thesis in your lab. Thanks for your always timely feedback and kind financial aid during my difficulty times.

PD Dr. Tobias Schiergens for being my supervisor. Your insightful feedback pushed me to sharpen my thinkings and brought my work to a higher level, your rigorousness and seriousness during our paper preparation as well as my dissertation revision impressed me a lot and would definitely have a very positive influence on my future journey. I also appreciate for all the trust, encouragement and kindness you have provided for me.

Dr. Serene Lee, thank you for all the technical support through the years, I have been touched by your thoughtful suggestions and kind words so many times.

PD Dr. Barbara Mayer, thank you for all the company during our working overtime and your patient answers no matter what I asked.

Prof. Dr. Jens H.L. Neumann, thank you for performing IHC staining and supporting me in the H&E slides, IHC slides and TILs score evaluation.

Prof. Christoph Becker and his team, Dr. Chen Varol and Frank Hipp, thanks for sharing your expertise, practical advices and kind support which provided me with a strong foundation to successfully establish the presented endoscopy aided CRC model.

Prof. Dr. Eckhard Wolf for kindly providing me with the MC38 cells.

Dr. Mehdi Shakarami and Dr. Barbara Eißner for your support during animal experiments. Your concern for animal welfare impressed me a lot and pushed me to invest more on

caring for the mice's well being during the *in vivo* experiments.

Ms. Edeltraud Hanesch for the assistance with graphics.

China Scholarship Council for honoring me the scholarship which covered all of my expenses in Germany for the first three years.

All the technicians in the lab for technical support and organizing a well-functioning lab, especially Sevdije Issar Amerchel, Nadine Gesse and Nicole Sylvia Strobl.

All the fellow students and former colleagues in the faculty for the help and pleasant working atmosphere, especially Dr. Sisi Lin, Dr. Zhiqiang Li, Dr. Jie Li, Yunjie Zhang, Huabin Zhang.

My sister Liangliang Nan, thanks for your financial support during my difficult times, and the stimulating discussions as well as happy distractions you provided to rest my mind outside of my research.

Finally my parents, for the endless love and support during all the stages of my education, thanks for your wise counsel, sympathetic ear and spiritual guidance.

Affidavit

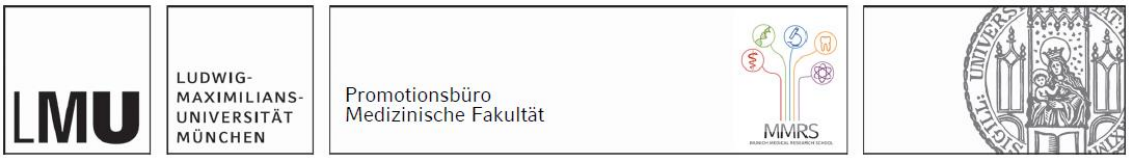

Affidavit

Chen, Chen

Surname, first name

Street

Zip code, town, country

I hereby declare, that the submitted thesis entitled:

Establishment of an Endoscopy-Guided minimally invasive
murine orthotopic colorectal cancer model

is my own work. I have only used the sources indicated and have not made unauthorised use of services of a third party. Where the work of others has been quoted or reproduced, the source is always given.

I further declare that the submitted thesis or parts thereof have not been presented as part of an examination degree to any other university.

München, 19.10.2021 — Chen Chen

place, date — Signature of the doctoral candidate

Confirmation of congruency

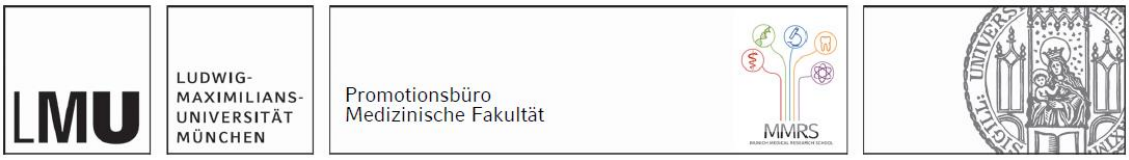

Confirmation of congruency between printed and electronic version of the doctoral thesis

Chen, Chen

Surname, first name

Street

Zip code, town, country

I hereby declare, that the submitted thesis entitled:

Establishment of an Endoscopy-Guided minimally invasive murine orthotopic colorectal cancer model

is congruent with the printed version both in content and format.

München, 19.10.2021 — Chen Chen

place, date — Signature of the doctoral candidate

List of publications

Chen C, Neumann J, Kühn F, Lee SML, Drefs M, Andrassy J, Werner J, Bazhin AV, Schiergens TS. Establishment of an Endoscopy-Guided Minimally Invasive Orthotopic Mouse Model of Colorectal Cancer. Cancers. 2020 Oct 12:3007.

Chen C, Dai P, Nan L, Lu R, Wang X, Tian Y, Zhang X, Gao Y, Zheng S, Zhang Y. Isolation and characterization of endothelial progenitor cells from canine bone marrow. Biotech Histochem. 2020 Jun 1:1-9.

Chen C, Tian Y, Wang J, Zhang X, Nan L, Dai P, Gao Y, Zheng S, Liu W, Zhang Y. Testosterone propionate can promote effects of acellular nerve allograft-seeded bone marrow mesenchymal stem cells on repairing canine sciatic nerve. J Tissue Eng Regen Med. 2019 Sep;13(9):1685-1701.

Chen C, Zheng S, Zhang X, Dai P, Gao Y, Nan L, Zhang Y. Transplantation of Amniotic Scaffold-Seeded Mesenchymal Stem Cells and/or Endothelial Progenitor Cells From Bone Marrow to Efficiently Repair 3-cm Circumferential Urethral Defect in Model Dogs. Tissue Eng Part A. 2018 Jan;24(1-2):47-56.